REPORT DOCUMENTATION PAGE

Form Approved OMB NO. 0704-0188

1. REPORT DATE (DD-MM-YYYY)	2. REPORT TYPE	3. DATES COVERED (From - To)
14-07-2015	Final Report	15-Jun-2011 - 14-Apr-2015

4. TITLE AND SUBTITLE
Final Report: Upconversion Effects in Resonantly Pumped Er3+ and Pr3+ Doped Low Phonon-Energy Crystals for Eye-Safe Laser Applications

5a. CONTRACT NUMBER
W911NF-11-1-0226

5b. GRANT NUMBER

5c. PROGRAM ELEMENT NUMBER
206022

6. AUTHORS
Althea G.Bluiett

5d. PROJECT NUMBER

5e. TASK NUMBER

5f. WORK UNIT NUMBER

7. PERFORMING ORGANIZATION NAMES AND ADDRESSES
Elizabeth City State University
1704 Weeksville Road

Elizabeth City, NC 27909 -9913

8. PERFORMING ORGANIZATION REPORT NUMBER

9. SPONSORING/MONITORING AGENCY NAME(S) AND ADDRESS (ES)
U.S. Army Research Office
P.O. Box 12211
Research Triangle Park, NC 27709-2211

10. SPONSOR/MONITOR'S ACRONYM(S)
ARO

11. SPONSOR/MONITOR'S REPORT NUMBER(S)
58939-EL-REP.9

12. DISTRIBUTION AVAILIBILITY STATEMENT
Approved for Public Release; Distribution Unlimited

13. SUPPLEMENTARY NOTES
The views, opinions and/or findings contained in this report are those of the author(s) and should not contrued as an official Department of the Army position, policy or decision, unless so designated by other documentation.

14. ABSTRACT
In this work, cw and pulsed ~ 1532 and ~ 1440 nm laser excitation of the 4I13/2 band of Er3+ and 3F3,3F4 band of Pr3+ was explored in low phonon-energy hosts KPb2Cl5 and KPb2Br5. Crystal growth along with upconversion and eye-safe emission (~ 1.5-1.6 μm) studies were conducted on both Er3+ and Pr3+ doped materials. Excitation spectra and emission decay transients of the infrared (4I9/2-->4I15/2) and green upconversion (2H11/2 + 4S3/2-->4I15/2) originating from Er3+ doped KPb2Cl5 and KPb2Br5 revealed that energy transfer upconversion (ETU) is the origin of the infrared and the green upconversion under 1532 nm excitation. Relative population calculations

15. SUBJECT TERMS
eye-safe laser materials, upconversion, rare-earth ions, energy transfer

16. SECURITY CLASSIFICATION OF:			17. LIMITATION OF ABSTRACT	15. NUMBER OF PAGES	19a. NAME OF RESPONSIBLE PERSON
a. REPORT	b. ABSTRACT	c. THIS PAGE			Althea Bluiett
UU	UU	UU	UU		19b. TELEPHONE NUMBER 252-335-3975

Report Title

Final Report: Upconversion Effects in Resonantly Pumped Er3+ and Pr3+ Doped Low Phonon-Energy Crystals for Eye-Safe Laser Applications

ABSTRACT

In this work, cw and pulsed ~ 1532 and ~ 1440 nm laser excitation of the 4I13/2 band of Er3+ and 3F3,3F4 band of Pr3+ was explored in low phonon-energy hosts KPb2Cl5 and KPb2Br5. Crystal growth along with upconversion and eye-safe emission (~ 1.5-1.6 μm) studies were conducted on both Er3+ and Pr3+ doped materials. Excitation spectra and emission decay transients of the infrared (4I9/2-->4I15/2) and green upconversion (2H11/2 + 4S3/2-->4I15/2) originating from Er3+ doped KPb2Cl5 and KPb2Br5 revealed that energy transfer upconversion (ETU) is the origin of the infrared and the green upconversion under 1532 nm excitation. Relative population calculations indicated that infrared upconversion is approximately two orders of magnitude stronger relative to the green upconversion. Interestingly, the upconversion microparameters for the infrared upconversion are very small having the values CDA ~ 3.5x10-42 cm6/s and CDA ~ 2.0x10-42 cm6/s for Er: KPb2Cl5 and Er: KPb2Br5, respectively. Due to the strong spectral overlap of the 4I13/2-->4I15/2 emission and 4I15/2 -->4I13/2 absorption bands Er-Er migration is believed to be assisting the energy transfer upconversion process in both Er: KPb2Cl5 and Er: KPb2Br5. Calculations indicated that the probability for energy migration is large yielding donor-donor critical radii of RDD ~ 16 Å and RDD ~ 17 Å for Er: KPb2Cl5 and Er: KPb2Br5, respectively, which are quite large but not unexpected due to the small stokes shifts between the 4I13/2-->4I15/2 emission band and 4I15/2-->4I13/2 absorption band of Er3+ in KPb2Cl5 and KPb2Br5. Visible upconversion was also observed in Pr3+ doped KPb2Cl5 and KPb2Br5 under ~ 1440 nm excitation where the emission originates from the 3P0, 3P1, and 1D levels. Emission decay measurements imply that ETU is the basis of the upconversion in Pr3+. Eye-safe emission (1.5-1.6 μm) arising from the 4I13/2-->4I15/2 of Er3+ and 3F3,3F4-->3H4 of Pr3+ accompanied upconversion and the relative population calculations for Er3+ indicated that both Er: KPb2Cl5 and Er: KPb2Br5 4I13/2-->4I15/2 infrared emission is dominant relative to the visible and infrared upconversion emission. Pr3+ doped in KPb2Cl5 and KPb2Br5 appears to be an attractive laser-ion given that upconversion seems to be less severe relative to Er3+ and in addition, it possesses superior absorption, emission and emission gain cross-sections relative to Er3+ doped in KPb2Cl5 and KPb2Br5.

Enter List of papers submitted or published that acknowledge ARO support from the start of the project to the date of this printing. List the papers, including journal references, in the following categories:

(a) Papers published in peer-reviewed journals (N/A for none)

Received	Paper

TOTAL:

Number of Papers published in peer-reviewed journals:

(b) Papers published in non-peer-reviewed journals (N/A for none)

Received		Paper
08/29/2014	4.00	Uwe Hommerich, Althea Bluiett, Courtney Kucera, Ei E. Brown, John Ballato , Sudhir Trivedi. Near Infrared and Upconversion Luminescence in Er:Y2O3 Ceramic under 1.5 um Excitation, J American Ceramic Society, (12 2013): 0. doi:
08/29/2014	6.00	U. Hömmerich, A.G. Bluiett , S.B. Trivedi, E. Brown, , E. Kumi-Barimah. Material purification, crystal growth, and spectroscopy of Tm-doped KPb2Cl5 and KPb2Br5 for 2 um photonic applications, Journa of Crystal Growth, (08 2013): 0. doi:
TOTAL:		**2**

Number of Papers published in non peer-reviewed journals:

(c) Presentations

(1) E. E. Brown, A. G. Bluiett, U. Hömmerich, S. B. Trivedi, Optical properties of Pr3+-, Ce3+-, and Eu3+-doped ternary lead halides, SPIE Photonics West Meeting, San Francisco California, Feb. 7 - 12, 2015.

(2) E. Brown, U. Hömmerich, A. C. Simmons1 B. Andrews, A G. Bluiett, and S. B. Trivedi, Growth and Optical Spectroscopy of Rare-Earth doped Potassium Lead Halides for potential applications in infrared lasers and radiation detectors, 20th American Conference on Crystal Growth and Epitaxy (ACCGE-20), August 2-7, 2015, Big Sky, Montana, submitted.

Number of Presentations: 2.00

Non Peer-Reviewed Conference Proceeding publications (other than abstracts):

Received		Paper
08/30/2013	1.00	. Upconversion and 1.5 μm - 1.6 μm infrared emission studies of Er3+ doped in the low phonon-energy hosts KPb2Cl5 and KPb2Br5 via 1.5 μm laser excitation, . , . : ,
TOTAL:		**1**

Number of Non Peer-Reviewed Conference Proceeding publications (other than abstracts):

Peer-Reviewed Conference Proceeding publications (other than abstracts):

Received		Paper
07/14/2015	8.00	Ei E. Brown , Althea Bluiett, Uwe Hömmerich, Sudhir B. Trivedi. Optical properties of Pr3+-, Ce3+-, and Eu3+-doped ternary lead halides, SPIE Photonics West. 07-FEB-15, . : ,
08/29/2014	5.00	Sudhir B. Trivedid, Olusola Oyebola, Ei E. Brown, Uwe Hömmerich, Althea Bluiett, Simone Hyater-Adams. Infrared Absorption and Fluorescence Propertiesof Ho-doped KPb2Br5, SPIE Photonics West. 02-FEB-14, . : ,
TOTAL:	**2**	

Number of Peer-Reviewed Conference Proceeding publications (other than abstracts):

(d) Manuscripts

Received		Paper
08/30/2013	3.00	. Material Purification, Crystal Growth, and Spectroscopy of Tm-doped KPb2Cl5 and KPb2Br5 for 2 μm Photonic Applications (SUBMITTED), ( )
TOTAL:	**1**	

Number of Manuscripts:

Books

Received	Book
TOTAL:	

Received	Book Chapter

TOTAL:

Patents Submitted

Patents Awarded

Awards

Graduate Students

NAME	PERCENT_SUPPORTED

FTE Equivalent:
Total Number:

Names of Post Doctorates

NAME	PERCENT_SUPPORTED

FTE Equivalent:
Total Number:

Names of Faculty Supported

NAME	PERCENT_SUPPORTED

FTE Equivalent:
Total Number:

Names of Under Graduate students supported

NAME	PERCENT_SUPPORTED	Discipline
Shevon Valinski	0.10	Biology
Terence Baker	0.20	Physics
Dylan Dutton	0.40	physics
Tahiya Manning	0.10	pharmaceutical Science
Shaunacee Howell	0.10	pharmaceutical Science
Ryans Onley	0.10	Biology
DeAndre McClary	0.10	Biology
Alexandria Leahy	0.10	Biology
Javaria Johnson	0.10	Chemistry
Ebrar Mohammad	0.10	Chemistry
Nigel Bethel	0.10	Biology
Joelle Dick	0.40	Physics
FTE Equivalent:	**1.90**	
Total Number:	**12**	

Student Metrics

This section only applies to graduating undergraduates supported by this agreement in this reporting period

The number of undergraduates funded by this agreement who graduated during this period: 5.00

The number of undergraduates funded by this agreement who graduated during this period with a degree in science, mathematics, engineering, or technology fields:..... 5.00

The number of undergraduates funded by your agreement who graduated during this period and will continue to pursue a graduate or Ph.D. degree in science, mathematics, engineering, or technology fields:..... 1.00

Number of graduating undergraduates who achieved a 3.5 GPA to 4.0 (4.0 max scale):..... 0.00

Number of graduating undergraduates funded by a DoD funded Center of Excellence grant for Education, Research and Engineering:..... 0.00

The number of undergraduates funded by your agreement who graduated during this period and intend to work for the Department of Defense 0.00

The number of undergraduates funded by your agreement who graduated during this period and will receive scholarships or fellowships for further studies in science, mathematics, engineering or technology fields:..... 0.00

Names of Personnel receiving masters degrees

NAME
Total Number:

Names of personnel receiving PHDs

NAME
Total Number:

Names of other research staff

NAME	PERCENT_SUPPORTED
FTE Equivalent:	
Total Number:	

Sub Contractors (DD882)

Inventions (DD882)

Scientific Progress

Attached

Technology Transfer

Upconversion Effects in Resonantly Pumped Er^{3+} and Pr^{3+} Doped Low Phonon-Energy Crystals for Eye-Safe Laser Applications

(Grant Number: W911NF-11-1-0026)

Dr. Althea G. Bluiett
Associate Professor of Physics
Phone: 252-335-3975
Fax: 252-335- 3508
Email: ablulett@mail.ecsu.edu
Elizabeth City State University
Department of Chemistry, Geology and Physics
Jenkins Science Building Room 404
1704 Weeksville Road
Elizabeth City, NC 27909

TABLE OF CONTENTS

Page

I. STUDENT RESEARCH AND OUTREACH ACTIVITIES..... 3
II. ABSTRACT.....8
III. INTRODUCTION 8
IV. EXPERIMENTAL CONDITIONS 9
V. CRYSTAL GROWTH.....9
VI. ABSORPTION COEFFICIENT OF Er^{3+} AND Pr^{3+} DOPED IN
KPb_2Cl_5 AND KPb_2Br_5.....10
VII. OPTICAL EMISSION AND ABSORPTION SPECTROSCOPY OF
Er^{3+} DOPED IN KPb_2Cl_5 AND KPb_2Br_5 11
A. Room Temperature Measurements.....11
B. Temperature Dependent Measurements.....20
VIII. OPTICAL EMISSION AND ABSORPTION SPECTROSCOPY OF
Pr^{3+} DOPED IN KPb_2Cl_5 AND KPb_2Br_5.....22
IX. INFRARED (1.5-1.6 μm) GAIN CROSS-SECTION FOR Pr^{3+} AND Er^{3+}.....29
X. CONCLUSIONS.....30
XI. REFERNCES…….....32

I. Student Research and Outreach Activities

The PI trained a number of students (e.g. figures 1a, 1b and 1c) to conduct basic spectroscopic measurements on Er: KPb_2Cl_5 and Er: KPb_2Br_5 crystals and present work at meetings. In addition, the students were informed on how to purify and grow these materials via visiting the crystal growth facility at Hampton University.

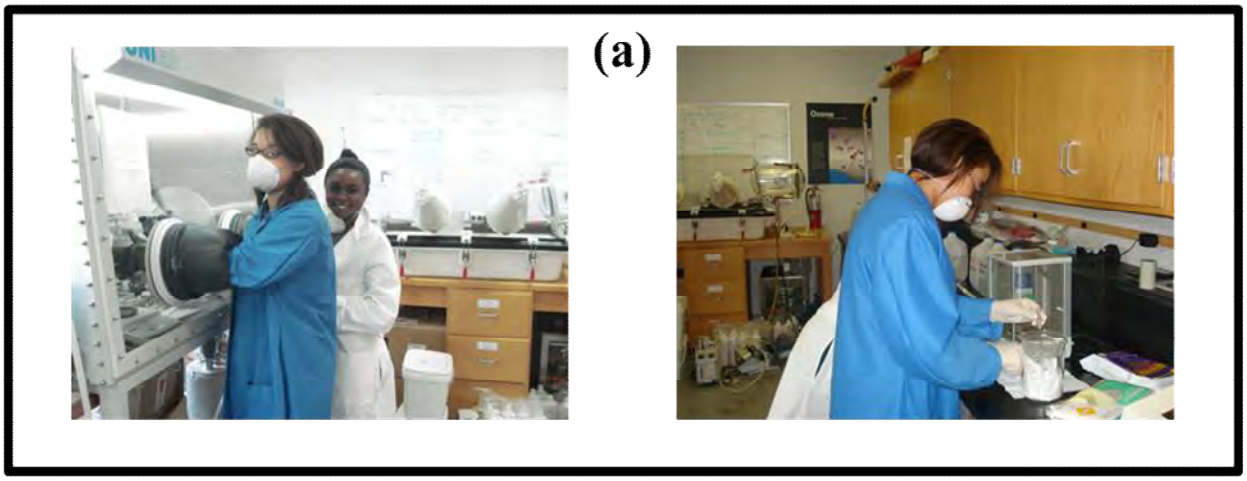

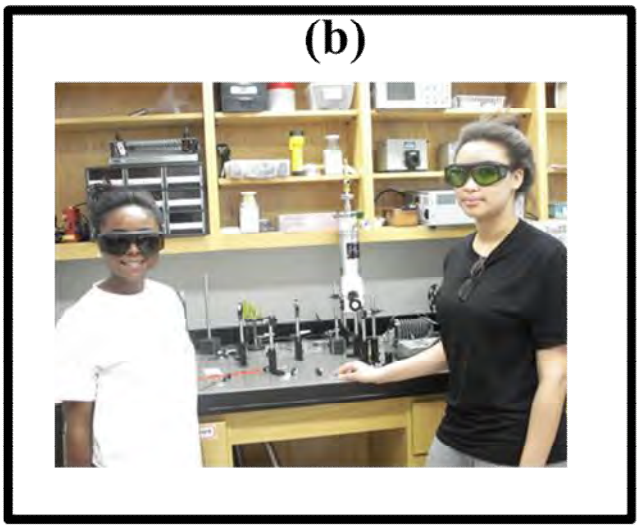

Figure 1 (a) Joelle Dick and Raven Wright are weighing purified KPb_2Cl_5 and $ErCl_3$ (in glove box) for loading into a cleaned quartz ampoule for crystal growth of Er: KPb_2Cl_5. (b) Students aligning experimental setup for spectral emission studies of Er: KPb_2Cl_5.

Outreach activities related to alternative energy was carried out by the P.I. (Dr. Althea G. Bluiett) along with undergraduate Elizabeth City State University (ECSU) students. These students were involved with

constructing and setting up the demonstrations and traveling with me to visit K-12 students. The goal of this project was to inform and garner interests as well as excitement in science in K-12 students via hands on activities and demonstrations. The hands-on activities included the following: building a hand electric generator, building an electric motor, producing hydrogen gas to operate a fuel cell car, and producing electricity using a bicycle generator. The demonstrations/hands-on activities are reusable and therefore can supplement physics lectures and laboratories which impacts ECSU undergraduate STEM students as well as summer high school and middle students who participate in summer programs at ECSU. I participated in Port Discover's Earth Day festival in Elizabeth City, North Carolina (figure 2). This occasion celebrates our planet Earth and informs the community on how to be more "green". My part in

Figure 2. Earth Day Festival in Elizabeth City, North Carolina

this festival was to inform the community on alternative forms of energy which involved employing two bicycle electric generators to convert a child's energy of motion into electricity which powered a slot-car, mini ferris-wheel, and a radio. To make the activities more interesting, a voltmeter was attached to the bicycle generator so that children could compete on who can produce the most voltage while pedaling the bicycle. In addition, ECSU students introduced the children to the mechanism behind an electric generator via dissecting a hand electric generator and identifying the basic components required to produce electricity. Listed below are other groups of K-12 students that were also impacted by the Department of Defense (DoD) funds:

(1) Elementary students at the Museum of the Albemarle during the spring 2013 (figure 3a)
(2) Elementary students at Port Discover during the spring of 2013 (figure 3b)
(3) Warren County middle school students visited ECSU during the fall of 2013 (figure 4)
(4) Elementary kids at Port Discover Summer Camp during the summer of 2014 (figure 5)
(5) Children's program at Pasquotank County Library during the summer of 2014 (figure 6)
(6) Girl's Incorporated of the Albemarle during the summer of 2014 (figure 7).

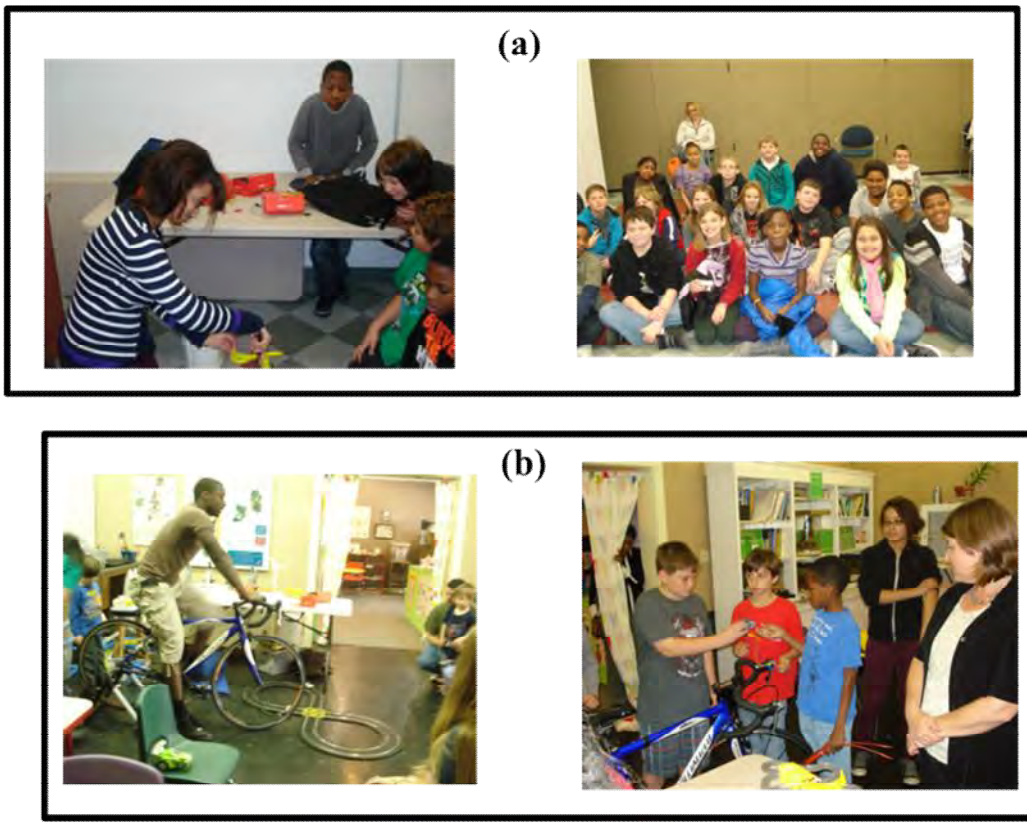

Figure 3. (a) Joelle Dick is demonstrating how liquid nitrogen shrinks a balloon by the extremely cold temperature reducing air pressure against its wall. (b) Terrance Pearson is demonstrating how we can convert mechanical energy into electricity via a bicycle generator.

Figure 4. Warren County Middle school children.

Figure 5. Port Discover Science Camp.

Figure 6. Children's Program at Pasquotank County Library.

Figure 7. Girls Incorporated of the Albemarle.

II. ABSTRACT

In this work, cw and pulsed ~ 1532 and ~ 1440 nm laser excitation of the $^4I_{13/2}$ band of Er^{3+} and $^3F_3$,$^3F_4$ band of Pr^{3+} was explored in low phonon-energy hosts KPb_2Cl_5 and KPb_2Br_5. Crystal growth along with upconversion and eye-safe emission (~ 1.5-1.6 μm) studies were conducted on both Er^{3+} and Pr^{3+} doped materials. Excitation spectra and emission decay transients of the infrared ($^4I_{9/2}$-->$^4I_{15/2}$) and green upconversion ($^2H_{11/2}$ + $^4S_{3/2}$-->$^4I_{15/2}$) originating from Er^{3+} doped KPb_2Cl_5 and KPb_2Br_5 revealed that energy transfer upconversion (ETU) is the origin of the infrared and the green upconversion under 1532 nm excitation. Relative population calculations indicated that infrared upconversion is approximately two orders of magnitude stronger relative to the green upconversion. Interestingly, the upconversion microparameters for the infrared upconversion are very small having the values $C_{DA} \sim 3.5x10^{-42}$ cm^6/s and $C_{DA} \sim 2.0x10^{-42}$ cm^6/s for Er: KPb_2Cl_5 and Er: KPb_2Br_5, respectively. Due to the strong spectral overlap of the $^4I_{13/2}$→$^4I_{15/2}$ emission and $^4I_{15/2}$ →$^4I_{13/2}$ absorption bands Er-Er migration is believed to be assisting the energy transfer upconversion process in both Er: KPb_2Cl_5 and Er: KPb_2Br_5. Calculations indicated that the probability for energy migration is large yielding donor-donor critical radii of $R_{DD} \sim 16$ Å and $R_{DD} \sim 17$ Å for Er: KPb_2Cl_5 and Er: KPb_2Br_5, respectively, which are quite large but not unexpected due to the small stokes shifts between the $^4I_{13/2}$→$^4I_{15/2}$ emission band and $^4I_{15/2}$→$^4I_{13/2}$ absorption band of Er^{3+} in KPb_2Cl_5 and KPb_2Br_5. Visible upconversion was also observed in Pr^{3+} doped KPb_2Cl_5 and KPb_2Br_5 under ~ 1440 nm excitation where the emission originates from the $^3P_0$, $^3P_1$, and ^1D levels. Emission decay measurements imply that ETU is the basis of the upconversion in Pr^{3+}. Eye-safe emission (1.5-1.6 μm) arising from the $^4I_{13/2}$→$^4I_{15/2}$ of Er^{3+} and $^3F_3$,$^3F_4$→$^3H_4$ of Pr^{3+} accompanied upconversion and the relative population calculations for Er^{3+} indicated that both Er: KPb_2Cl_5 and Er: KPb_2Br_5 $^4I_{13/2}$→$^4I_{15/2}$ infrared emission is dominant relative to the visible and infrared upconversion emission. Pr^{3+} doped in KPb_2Cl_5 and KPb_2Br_5 appears to be an attractive laser-ion given that upconversion seems to be less severe relative to Er^{3+} and in addition, it possesses superior absorption, emission and emission gain cross-sections relative to Er^{3+} doped in KPb_2Cl_5 and KPb_2Br_5.

III. INTRODUCTION

Efficient laser emission in the 1.5 – 1.6 μm eye-safe wavelength window continues to be of significant interest for civilian and military applications [1-4]. Solid-state lasers based on the laser ion Er^{3+} have been extensively investigated in YAG as well as the sesquioxides and glass hosts whose inter-manifold $^4I_{13/2}$→$^4I_{15/2}$ laser transition conveniently overlaps the eye-safe wavelength window. The main issue with the fabrication of an efficient Er^{3+}solid-state laser system is the thermal loads that accompany the pumping of the crystal. To reduce the effects of heat production extensive research is currently being conducted on resonantly pumped Er^{3+}via 1.5 μm laser excitation [1-5]. Resonant excitation of Er^{3+} essentially refers to direct excitation of Er^{3+} ions to the upper laser level. This excitation pathway is currently being exploited for the difference in energy between the pump and laser wavelengths leads to less quantum defect heating. Though, resonant pumping scheme is motivated by reduced quantum defect heating, resonant pumping of Er^{3+} suffers from the deleterious effects of energy transfer upconversion (ETU), which is an additional channel for adding heat into the crystal. Furthermore, ETU removes population from the upper laser level [6-9] which increases laser pump threshold. In addition to ETU, upconversion due to excited state absorption (ESA) of the pump can add on to the thermal load. To minimize the effects of upconversion, incorporating Er^{3+} into relatively new solid-state gain media the ternary lead halides (KPb_2Cl_5, KPb_2Br_5, and $RbPb_2Cl_5$) is of interest [8]. Er^{3+} upconversion has been reported in KPb_2Cl_5 and KPb_2Br_5 as well as other low phonon-energy hosts under ~980 nm or ~800 nm laser excitation [10,11,12,13,14,15]. However, less work has been reported on the upconversion dynamics under resonant pumping of the $^4I_{13/2}$ absorption band of Er^{3+} in low phonon-energy hosts [8,16]. In this study we will explore the Er^{3+}upconversion and 1.5 μm eye-safe emission in KPb_2Cl_5 and KPb_2Br_5 under ~ 1532 nm laser excitation. In addition to Er^{3+}, triply ionized praseodymium has been extensively

investigated in glass hosts and crystals because of its multiple metastable states in the visible wavelength region. Incorporating Pr^{3+} in low phonon energy hosts such as $LaCl_3$, KPb_2Cl_5, KPb_2Br_5 and $RbPb_2Cl_5$ allows the possibility to extend the metastable states into the mid-infrared regime. For instance, lasing between 1.3-7.2 μm from Pr^{3+} has been demonstrated in the low phonon energy host $LaCl_3$ [17,18] and lasing between 2.3 – 2.5 μm [19] in Pr: $RbPb_2Cl_5$ was demonstrated. Very recently, 1.6 μm lasing originating from resonantly pumped Pr^{3+} in the low-phonon energy host $RbPb_2Cl_5$ was reported at cryogenic temperature [20]. Stimulated by these results there is interest in exploiting the $^3F_3$,$^3F_4 \rightarrow {}^3H_4$ 1.6 μm transition of Pr^{3+} in KPb_2Cl_5 and KPb_2Br_5 for this transition also overlap the eye-safe wavelength window (1.5 – 1.6 μm). In this report a comparative study of the spectroscopic characteristics of resonantly pumped Er^{3+} and Pr^{3+} singly doped in the low phonon-energy hosts $KPb_2Cl_5$and KPb_2Br_5will be discussed.

IV. Experimental Conditions

The absorption spectra for the investigated samples were collected by either utilizing a Nicolet 6700 Fourier-transform infrared spectrometer or a Cary 5000 spectrophotometer. The emission spectra were generated by pumping the $^4I_{13/2}$ absorption band of Er^{3+} with an Er-fiber laser operating at approximately 1532 nm, whereas the $^3F_3$,$^3F_4$ absorption band of $Pr^{3+}$was pumped by exciting it with ~1440 nm line from a diode laser. Spectral response of the experimental setup was corrected by employing a quartz tungsten halogen calibration lamp from Newport Corporation. The ~1505 nm and 1436 nm outputs of Nd: YAG pumped optical parametric oscillator system (5 ns pulses, 10 Hz) were utilized for 1.5-1.6 μm infrared emission decay measurements of Er^{3+} and Pr^{3+}, respectively. Both temporal and spectral visible upconversion emission from Pr^{3+}were generated by employing a Nd: YAG pumped OPO operating at ~1550 nm and direct visible emission spectra and decay transients were produced by tuning the OPO to 474 nm and 590 nm. Excitation spectra were collected by exciting Er^{3+} at a range of wavelengths overlapping the $^4I_{13/2}$ absorption band via the idler beam of a Nd:YAG pumped OPO and processed using a boxcar averaging system. Low temperature measurements were conducted using a two-stage closed-cycle helium refrigerator.

V. Crystal Growth

The growth of Er: KPb_2Cl_5, Er: KPb_2Br_5, Pr: KPb_2Cl_5 and Pr:KPb_2Br_5 is highly dependent on the quality of the starting materials (KCl, KBr, $PbCl_2$, $PbBr_2$, $PrCl_3$, $PrBr_3$, $ErCl_3$ and $ErBr_3$) that is purchased commercially. Because of this, stoichiometric amounts of ultra-dry, high purity materials were purchased from Alpha Aesar and accurately measured inside an argon-purged glove-box and loaded into a thoroughly cleaned and baked quartz ampoule. Even though commercially purchased materials are ultra-dry, there could still remain traces of water as well as oxidic impurities that must be removed. These impurities will be embedded in the melt and will hinder normal growth of single crystals, and can possibly function as emission quenching centers. Consequently, the loaded ampoule of starting material was initially dried under vacuum at ~120^o C and ~ 10^{-5} Torr for 24 hours and then vacuum sealed. The material was then melted and purified via 10-15 uni-direction translation within a zone-refiner, where most of the impurities drifted to the ends of the ampoule and the middle portion of the synthesized material was free from oxide and lead impurities. The dopant materials $PrCl_3$, $PrBr_3$, $ErCl_3$ and $ErBr_3$ also hydrolyzes in the presence of moisture and was purified through a similar zone-refinement technique as well. To synthesize the rare-earth doped chloride and bromide materials purified KPb_2Cl_5, KPb_2Br_5, and dopant materials were initially melted in an argon (or nitrogen gas) environment for ~ 1 hour. To minimize the decomposition of the material into lead impurities, the material was chlorinated or brominated via bubbling HCl or HBr gas into the melt for 3 hours using small capillary tubing. This was followed by flushing the material with argon gas (or nitrogen gas) and then rapidly cooling to room temperature. The chlorinated or brominated material was loaded into a new ampoule and grown via

modified Bridgman growth. Figure 8 displays polished samples of Er: KPb_2Cl_5, Er: KPb_2Br_5, and Pr: KPb_2Br_5.

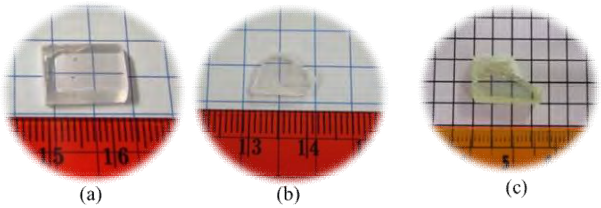

Figure 8. Polished samples of (a) Er: KPb_2Cl_5, (b) Er: KPb_2Br_5, and (c) Pr: KPb_2Br_5 grown at Hampton University.

VI. Absorption Coefficient of Er^{3+} and Pr^{3+} Doped in KPb_2Cl_5 and KPb_2Br_5

Figure 9 displays the intra-4f absorption bands of Er: KPb_2Cl_5 and Er: KPb_2Br_5 crystals measured between 400 – 1800 nm. The lowest-lying band is centered ~ 6700 cm^{-1} ($^4I_{13/2}$) above the ground state, providing a channel for 1.5 μm eye-safe emission. This band is strongly coupled to 1.5 μm diode laser sources which allows for an efficient pumping scheme. The two crystals under study have similar Er-ion concentrations of $5.3x10^{19}$ cm^{-3} and $4.1x10^{19}$ cm^{-3} for Er: KPb_2Cl_5 and Er: KPb_2Br_5, respectively. The absorption cross-sections at the 1532 nm pump wavelength are ~ $0.6x10^{-20}$ cm^2 and ~ $0.8x10^{-20}$ cm^2 for Er: KPb_2Cl_5 and Er: KPb_2Br_5, respectively. Depicted in figures 10a and 10b are the intra-4f absorption bands from Pr: KPb_2Cl_5

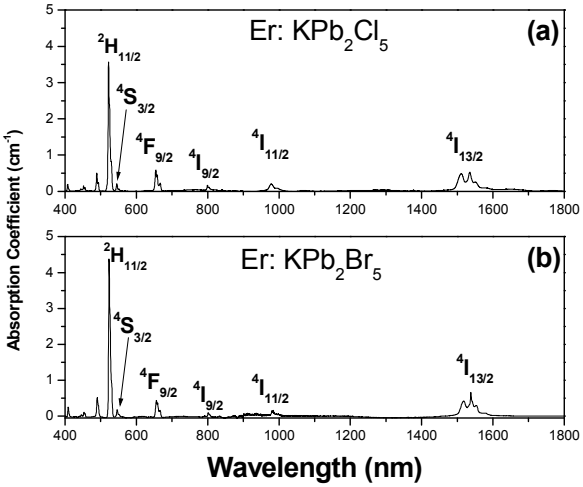

Figure 9. Unpolarized, room temperature absorption coefficient spectra of (a) Er: KPb_2Cl_5 and (b) Er: KPb_2Br_5.

and Pr: KPb_2Br_5, respectively. The $^3F_3$+$^3F_4$ absorption band is of interest for pumping Pr^{3+} in the hopes for efficient eye-safe emission in the 1.5-1.6 μm range. The absorption cross-sections at the 1532 nm pump wavelength are ~ $1.4x10^{-20}$ cm^2 and ~ $0.78x10^{-20}$ cm^2 for Pr: KPb_2Cl_5 and Pr: KPb_2Br_5, respectively.

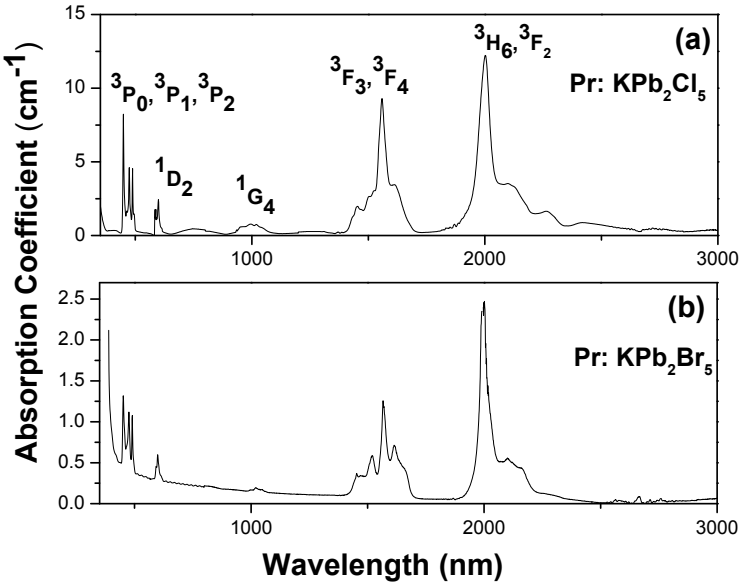

Figure 10. Unpolarized, room temperature absorption coefficient spectra of (a) Pr: KPb_2Cl_5 and (b) Pr: KPb_2Br_5.

VII. Optical Emission and Absorption Spectroscopy of Er^{3+} Doped in KPb_2Cl_5 and KPb_2Br_5

A. Room Temperature Measurements

Figures 11a and 11b present the room temperature, blackbody corrected $^4I_{13/2} \rightarrow {}^4I_{15/2}$ emission cross-sections arising from both Er: KPb_2Cl_5 and Er: KPb_2Br_5, as well as their respective $^4I_{15/2} \rightarrow {}^4I_{13/2}$ absorption cross-sections. The emission cross-sections were calculated using the Füchtbauer-Landenburg relation [21,22]:

$$\sigma_{Emiss} = \frac{1}{8\pi n^2 c}\frac{\beta}{\tau_{Rad}}\frac{\lambda^5 I(\lambda)}{\int \lambda I(\lambda) d\lambda} \tag{1}$$

where, c is the speed of light, n is the index of refraction of the crystal and τ_{Rad} is the radiative emission decay time. The absorption cross-sections were determined by dividing the absorption coefficient by their respective Er^{3+} ion concentrations. The emissions were generated by exciting Er^{3+} with ~140 mW of 1532 nm laser excitation. To visualize the entire $^4I_{13/2} \rightarrow {}^4I_{15/2}$ emission band free from laser scattering the emission spectra were measured under both 970 nm and 1532 nm laser excitation and then the two spectra were joined together. This is necessary for the 1532 nm pump wavelength is coupled to the $^4I_{13/2} \rightarrow {}^4I_{15/2}$ emission band of Er^{3+}. As can be observed in figure 11 the emission spectra are weakly stokes shifted from their respective absorption spectrum, which is characteristic for trivalent rare earth ions doped in solid-state hosts materials. The peak emission cross-section of Er^{3+}does not vary significantly between the two hosts KPb_2Cl_5 ($\sigma_{1537\ nm}$ ~ 0.9 cm^2) and KPb_2Br_5 ($\sigma_{1540\ nm}$ ~ 1.6cm^2) and in fact have values similar to Er: YAG ($\sigma_{1537\ nm}$ ~ 1.7 cm^2). The overall dominant emission under resonant 1.5 μm pumping of both

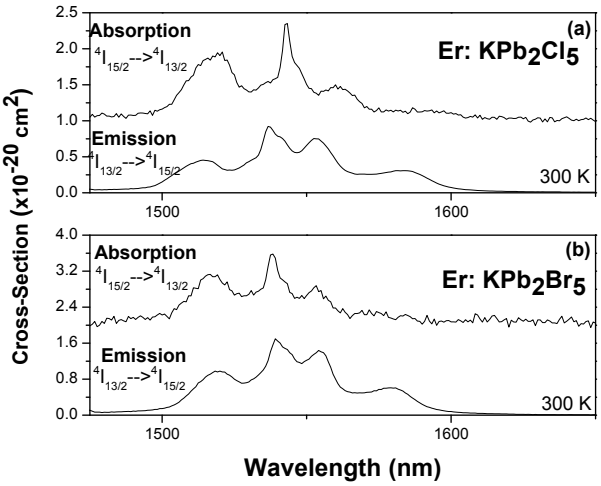

Figure 11. Room temperature absorption and emission cross-sections from (a) Er: KPb_2Cl_5 and (b) Er: KPb_2Br_5.

Er: KPb_2Cl_5 and Er: KPb_2Br_5 stems from the $^4I_{13/2} \rightarrow {}^4I_{15/2}$ stoke emission. As is well understood, resonantly pumping Er^{3+} via ~1500 nm laser excitation is of current interest for 1.5-1.6 μm eye-safe laser applications for the inherently smaller quantum defect between the pump and the laser wavelength automatically reduces heat deposition into the crystal. However, due to the resonances within the energy levels of Er^{3+}, other channels of heat production arises through the well-known upconversion processes. Consequently, besides the 1.5 μm stokes emission, upconversion emission (also known as anti-stokes emission) was also observed in the infrared as well as in the visible regime. The dominant upconversion emission is in the infrared and corresponds to the $^4I_{9/2} \rightarrow {}^4I_{15/2}$ transition of Er^{3+} and peaks at ~ 805 and 807 nm for Er: KPb_2Cl_5 and Er: KPb_2Br_5, respectively (figure 12). A weaker infrared upconversion emission band corresponding to the $^4S_{3/2} \rightarrow {}^4I_{13/2}$ transition of Er^{3+} peaks at 856 nm and 858 nm for Er: KPb_2Cl_5 and Er: KPb_2Br_5, respectively (figure 12). The dominant $^4I_{9/2} \rightarrow {}^4I_{15/2}$ infrared upconversion is typical in low phonon-energy hosts. For example, under similar pumping conditions, Er: Yttria dominant upconversion transition is not the $^4I_{9/2} \rightarrow {}^4I_{15/2}$ but rather the visible transitions (figure 13). This observation is due to the fact that Yttria has larger phonon energy (~ 450-550 cm^{-1}) relative to KPb_2Cl_5 (~ 203 cm^{-1}) and KPb_2Br_5 (~ 138 cm^{-1}) and therefore multiphonon emission from the $^4I_{9/2}$ is more competitive. In even larger phonon energy hosts such as YAG the $^4I_{9/2} \rightarrow {}^4I_{15/2}$ upconversion is negligible. The most intense visible upconversion emission arising from Er: KPb_2Cl_5 and Er: KPb_2Br_5 is green and stems from the $^4S_{3/2} \rightarrow {}^4I_{15/2}$ transitions of Er^{3+} and peaks at ~ 548 nm for both Er: KPb_2Cl_5 and Er: KPb_2Br_5. A second, weaker green

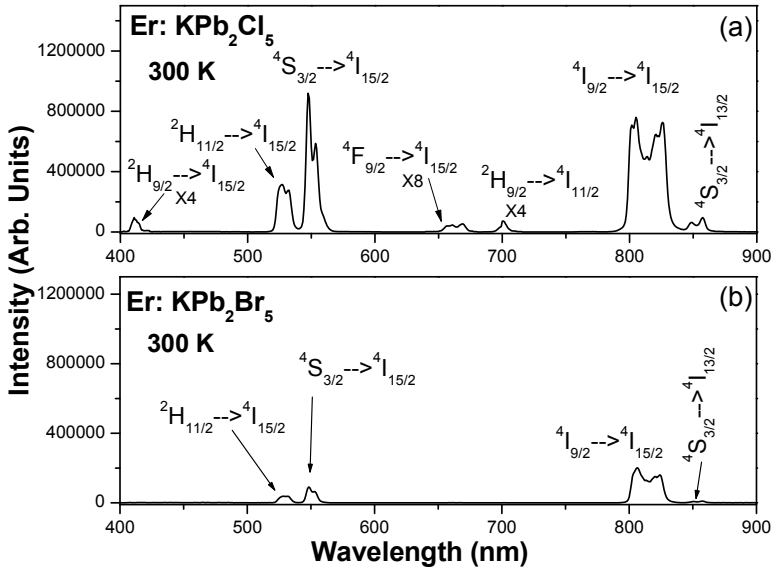

Figure 12. Room temperature emission from (a) Er: KPb_2Cl_5 and (b) KPb_2Br_5 stimulated by 1532 nm cw laser excitation.

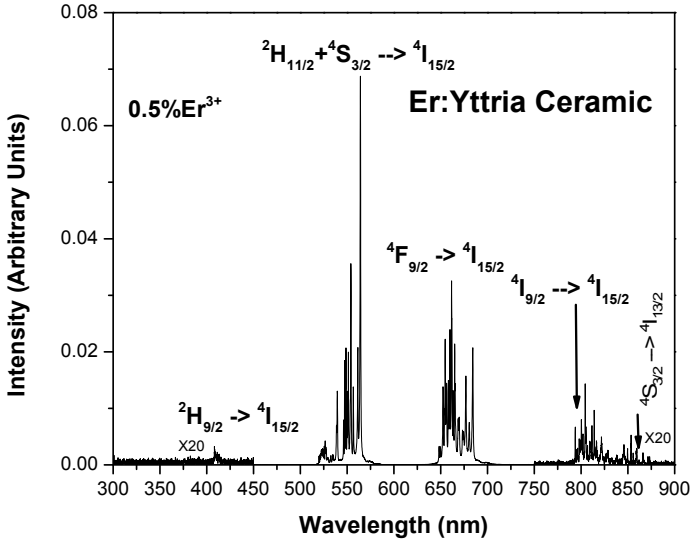

Figure 13. Room temperature emission from Er: Yttria ceramic.

upconversion emission band $^2H_{11/2} \rightarrow {}^4I_{15/2}$ was also observed and is situated at 527 and 528 nm in Er: KPb_2Cl_5 and Er: KPb_2Br_5, respectively. The $^2H_{11/2}$ is only ~800 cm^{-1} above the $^4S_{3/2}$ and can be bridged by high frequency phonons, consequently the $^2H_{11/2}$ and $^4S_{3/2}$ are thermally coupled at room temperature. Thus, at 300 K these two states will be treated as one state and will be labeled as $^2H_{11/2}+{}^4S_{3/2}$. Considerably weaker red upconversion at ~ 669 nm ($^4F_{9/2} \rightarrow {}^4I_{15/2}$) and blue upconversion at ~ 411 nm

($^2H_{9/2}\rightarrow{}^4I_{15/2}$) were also observed and was more pronounced in Er: KPb_2Cl_5. It should be mentioned that the intensity of the blue emission was limited by the spectral response of the experimental setup. However, the blue emission is typically weaker under excitation of the $^4I_{13/2}$ band of Er^{3+} [2]. Consequently, the blue and red upconversion emission will not be discussed any further. As mentioned earlier the most dominant upconversion emission at 300 K from Er: KPb_2Cl_5 and Er: KPb_2Br_5 are the green ($^2H_{11/2}+{}^4S_{3/2}\rightarrow{}^4I_{15/2}$) and the infrared ($^4I_{9/2}\rightarrow{}^4I_{15/2}$). Similar observation was reported in the chloride-based host Er: $CsLu_2Cl_9$ [16] under resonant pumping of the $^4I_{13/2}$ band of Er^{3+}. To quantitate this observation the relative populations of the green emitting levels ($^2H_{11/2}$ + $^4S_{3/2}$) and the infrared emitting level ($^4I_{9/2}$) were calculated by using an expression from Quimby et al. [8]

$$\frac{R_{ni}}{R_{mj}}=\frac{N_n}{N_m}\frac{W_{ni}}{W_{mj}} \tag{2}$$

where $R_{ni}=\frac{\lambda}{hc}\int \lambda\, I_{ni}(\lambda)d\lambda$ and $R_{mi}=\frac{\lambda}{hc}\int \lambda\, I_{mi}(\lambda)d\lambda$ are the total photon emission rates stemming from the n→i and m→j emission transitions, respectively, the ratio $\frac{N_n}{N_m}$ are the average population of the n and m excited states, respectively, h is Planck's constant, and c is the speed of light. W_{ni} and W_{mj} are the radiative rates coming from the n→i and m→j emission transitions, respectively. The total relative photon emission rates were measured using the blackbody calibrated emission bands stemming from the $^4I_{9/2}\rightarrow{}^4I_{15/2}$ and $^2H_{11/2}$ + $^4S_{3/2}\rightarrow{}^4I_{15/2}$ transitions of Er: KPb_2Cl_5 and Er: KPb_2Br_5. Since the $^2H_{11/2}$ + $^4S_{3/2}$ are thermally coupled at 300 K the effective radiative rate was calculated using the following expression [23],

$$W_{eff}=\frac{g_H\exp(-E/KT)W_H+g_SW_S}{g_H\exp(-E/KT)+g_S} \tag{3}$$

where W_H and W_S are the radiative emission rate from the $^2H_{11/2}$ and $^4S_{3/2}$ levels, g_H and g_S are the degeneracies of the $^2H_{11/2}$ and $^4S_{3/2}$ levels, respectively, and E is the energy gap between the $^2H_{11/2}$ and $^4S_{3/2}$ levels. The relative population of the green and 800 nm infrared emitting levels (N_{Green}/N_{IR} nm) were determined to be ~ 0.04 and ~ 0.02 for Er: KPb_2Cl_5 and Er: KPb_2Br_5, respectively, when excited with a pump power of ~140 mW. This indicates that at moderate pumping power more Er^{3+} ions are elevated to the $^4I_{9/2}$ relative to the thermally coupled $^2H_{11/2}$ + $^4S_{3/2}$ levels in both the chloride and bromide based hosts. This observation is not unexpected since the $^2H_{11/2}$ + $^4S_{3/2}\rightarrow{}^4I_{15/2}$ upconversion is a higher order process, which results in smaller population density and therefore smaller population relative to the $^4I_{9/2}\rightarrow{}^4I_{15/2}$

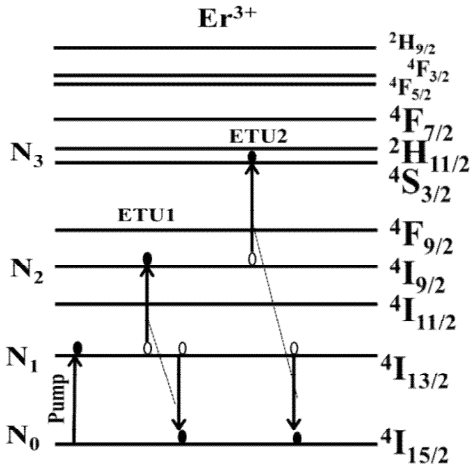

Figure 14. Schematic energy level diagram of Er^{3+}. The filled circles represent Er^{3+} population following 1532 nm laser excitation. The $^2H_{9/2}$ and $^4F_{9/2}$ also have some population but are weak and will therefore be neglected. The unfilled circles represent energy levels that were depopulated following ETU.

infrared upconversion. The relative populations of the $^4I_{9/2}$ and $^4I_{13/2}$ levels (N_{IR} nm /N_{1500}) were determined to be ~ 0.001 and ~ 0.0005 Er: KPb_2Cl_5 and Er: KPb_2Br_5, respectively, indicating that the majority of the absorbed 1532 nm pump photons contributes to the 1.5 μm emission. According to references [8] and [16] the infrared upconversion emitted in the 800 nm regime is attributed to a two-step process, ground state absorption of the pump ($^4I_{15/2}\rightarrow{}^4I_{13/2}$) followed by energy transfer upconversion ($^4I_{13/2}$,$^4I_{13/2}$)$\rightarrow$($^4I_{15/2}$,$^4I_{9/2}$) (fig. 14;ETU1). It should be emphasized that ETU1 process removes 2 electrons from the $^4I_{13/2}$ level which is undesirable for laser oscillation from the $^4I_{13/2}$. Due to ETU1 process ETU2/ESA process is now attainable and removes an additional electron from the $^4I_{13/2}$. This is possible because chloride and bromide based materials possess low phonon-energy and rapid multiphonon emission to the next lower level ($^4I_{11/2}$) after ETU1 is less efficient making the $^4I_{9/2}$ a metastable state and therefore an intermediate state for the green upconversion process via excited state absorption of the pump (Pump + $^4I_{9/2}\rightarrow{}^2H_{11/2}$ + $^4S_{3/2}$) and/or energy transfer upconversion ($^4I_{9/2}$,$^4I_{13/2}$)$\rightarrow$($^2H_{11/2}$ + $^4S_{3/2}$, $^4I_{15/2}$) (fig. 14; ETU2) [2,3]. A technique commonly used to decipher if ETU or ESA is populating upper energy levels involves comparing the excitation spectrum of the upconverted emission with the corresponding ground state absorption spectrum [10,11,15]. An indicator that ETU is active occurs when the excitation spectrum of the upconverted emission looks comparable to the corresponding ground state absorption spectrum [10,11,15]. Evidence of ESA occurs when the excitation spectrum of the upconverted emission possesses additional absorption peaks not seen in the corresponding ground state absorption band. These peaks represent additional absorption transition after ground state absorption [10,11,15]. Depicted in figures 15a and 15b are the 300 K excitation spectrum of the $^4I_{9/2}\rightarrow{}^4I_{15/2}$ and $^2H_{11/2}$ + $^4S_{3/2}\rightarrow{}^4I_{15/2}$ upconverted emissions from Er: KPb_2Cl_5 along with the $^4I_{15/2}\rightarrow{}^4I_{13/2}$ ground state absorption band of Er: KPb_2Cl_5. It is evident that the excitation spectra in figures 15a and 15b are very close to the $^4I_{15/2}\rightarrow{}^4I_{13/2}$ ground state absorption band of Er: KPb_2Cl_5 indicating that ETU is likely responsible for the population in

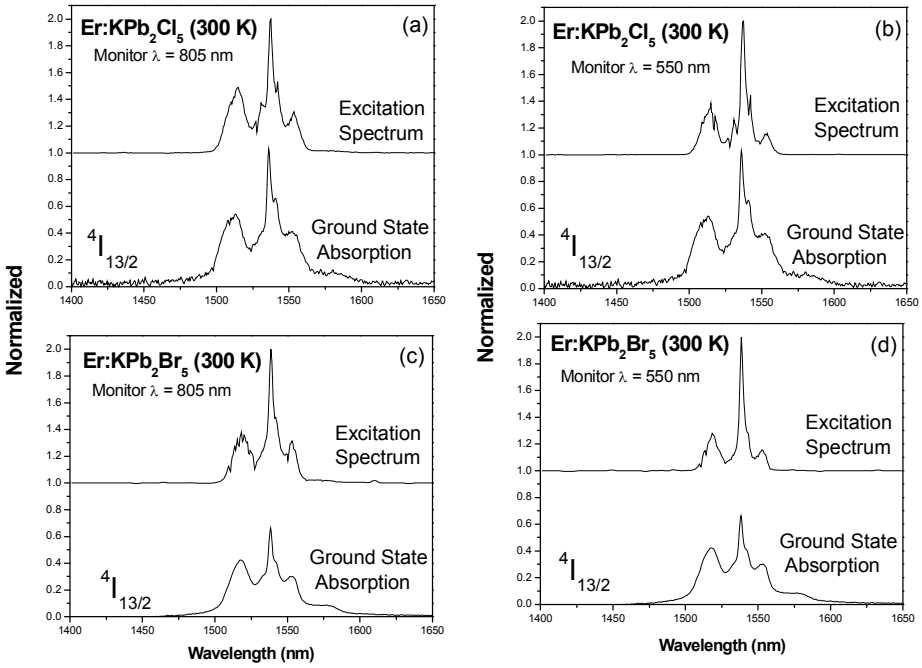

Figure 15. Room temperature excitation spectra of the upconverted emission from $^4I_{9/2} \rightarrow {}^4I_{15/2}$ of Er^{3+} overlaid with the 300K $^4I_{15/2} \rightarrow {}^4I_{13/2}$ ground state absorption band for (a) Er: KPb_2Cl_5 and (c) KPb_2Br_5. Room temperature excitation spectra of the upconverted emission from $^2H_{11/2}$ + $^4S_{3/2} \rightarrow {}^4I_{15/2}$ of Er^{3+} overlaid with the 300 K $^4I_{15/2} \rightarrow {}^4I_{13/2}$ ground state absorption band for (b) Er: KPb_2Cl_5 and (d) KPb_2Br_5.

the $^4I_{9/2}$ and the thermally coupled $^2H_{11/2}$ + $^4S_{3/2}$ levels rather than ESA. Figures 15c and 15d displays the excitation spectra of the $^4I_{9/2} \rightarrow {}^4I_{15/2}$ and $^2H_{11/2}$ + $^4S_{3/2} \rightarrow {}^4I_{15/2}$ upconverted emissions from Er: KPb_2Br_5 and the $^4I_{15/2} \rightarrow {}^4I_{13/2}$ ground state absorption band of Er: KPb_2Br_5. Similarly, the excitation spectra and the ground state absorption band of Er: KPb_2Br_5 are comparable which implies that ETU could be responsible for populating the $^4I_{9/2}$ and $^2H_{11/2}$ + $^4S_{3/2}$ levels. To further confirm the origin of the upconversion mechanisms, the decay transients of the upconverted emissions were collected. Figure 16a displays the $^4I_{9/2} \rightarrow {}^4I_{15/2}$ decay transients of Er: KPb_2Cl_5 and Er: KPb_2Br_5 after 1532 nm pulsed laser excitation (~5 ns). The transients show a rise time after the laser pulse followed by a decay time of $\tau \sim 5.9$ ms and $\tau \sim 4.2$ ms for Er: KPb_2Cl_5 and Er: KPb_2Br_5, respectively. The emission decay times are significantly longer relative to direct excitation of the $^4I_{9/2}$ ($\tau \sim 2.4$ ms [24] for Er: KPb_2Cl_5 and $\tau \sim 1.9$ ms [13] for Er: KPb_2Br_5). This feature is indicative of nonradiative ETU process taking place [16]. Furthermore, another characteristic

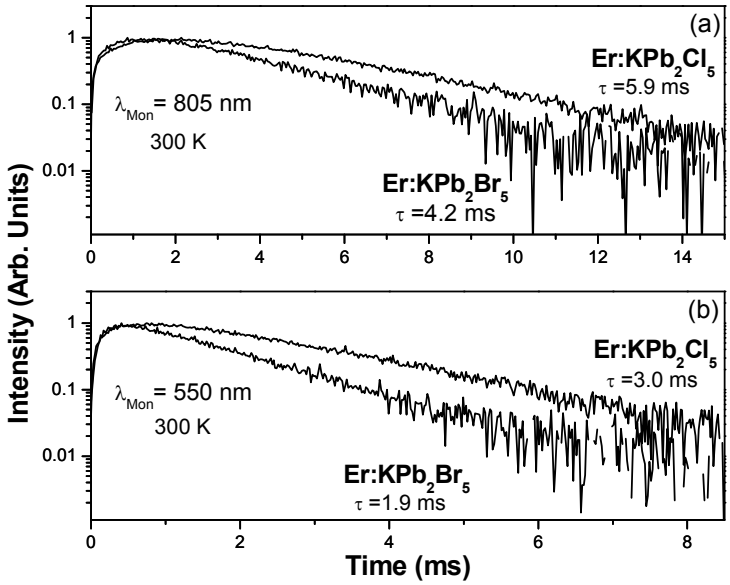

Figure 16. (a) Room temperature upconverted emission decay transients of the $^4I_{9/2} \rightarrow {}^4I_{15/2}$ of Er^{3+} from Er: KPb_2Cl_5 and Er: KPb_2Br_5. (b) Room temperature upconverted emission decay transients of the $^2H_{11/2} + {}^4S_{3/2} \rightarrow {}^4I_{15/2}$ of Er^{3+} from Er: KPb_2Cl_5 and Er: KPb_2Br_5.

of ETU is that the decay time of the upconverted emission corresponds to the decay time of the intermediate state [16]. As just mentioned, the decay time of the upconverted $^4I_{9/2} \rightarrow {}^4I_{15/2}$ emission from Er: KPb_2Cl_5 and Er: KPb_2Br_5 are 5.9 ms and 4.2 ms, which are very close to the decay time of the intermediate state ($^4I_{13/2}$) which are 4.2 ms [24] and 4.6 ms [13], respectively. In the case of the radiative ESA process, the decay occurs immediately after the laser pulse given that ESA occurs only during the laser pulse. The decay time of the upconverted emission via ESA is similar to the decay time after direct laser excitation [11,16]. Displayed in figure 16b are the decay transients of the $^2H_{11/2} + {}^4S_{3/2} \rightarrow {}^4I_{15/2}$ emission, where there is a rise time after the laser pulse followed by a decay times of $\tau \sim 3.1$ ms and $\tau \sim 1.9$ ms for Er: KPb_2Cl_5 and Er: KPb_2Br_5, respectively. The emission decay times are significantly longer relative to direct excitation of the $^2H_{11/2} + {}^4S_{3/2}$ ($\tau \sim 238$ μs [11] for Er: KPb_2Cl_5 and $\tau \sim 180$ μs [13] for Er: KPb_2Br_5). It has been reported that excited state absorption is likely the mechanism responsible for the green upconversion in Er: KPB_2Cl_5under excitation of the $^4I_{13/2}$ [8], however the decay transient in figure 16b along with the excitation spectrum of the $^2H_{11/2} + {}^4S_{3/2} \rightarrow {}^4I_{15/2}$ upconverted emission from Er: KPb_2Cl_5 suggests that ETU is responsible for populating the $^2H_{11/2} + {}^4S_{3/2} \rightarrow {}^4I_{15/2}$ levels for both the chloride as well as the bromide hosts. In addition, the decay time of the upconverted $^2H_{11/2} + {}^4S_{3/2} \rightarrow {}^4I_{15/2}$ emission from Er: KPb_2Cl_5 and Er: KPb_2Br_5 are 3.0 ms and 1.9 ms, which are very close to the decay time of the intermediate state ($^4I_{9/2}$) which are 2.4 ms [11] and 1.9 ms [13], respectively. Consequently, population within the $^4I_{9/2}$ and $^2H_{11/2} + {}^4S_{3/2}$ levels are assigned to the energy transfer upconversion processes ($^4I_{13/2}$, $^4I_{13/2}) \rightarrow (\ ^4I_{15/2}$, $^4I_{9/2})$ and ($^4I_{13/2}$, $^4I_{9/2}) \rightarrow (\ ^4I_{15/2}$, $^2H_{11/2} + {}^4S_{3/2})$, respectively. Due to the observed energy mismatch between the donor and acceptor transitions the energy transfer processes are nonresonant. In addition, this nonresonant process is exothermic in nature indicating that the donor ions transition energy is greater than the acceptor ion transition energy and therefore phonon emission accompanies the energy transfer and has a relatively higher probability of occurring compared to an endothermic phonon absorbing process [25]. From the spectroscopic data the energy mismatches for Er: KPb_2Cl_5 were approximated to be $\Delta E \sim 680$ cm^{-1} and $\Delta E \sim 590$ cm^{-1} for ETU1 and ETU2, respectively, and for Er: KPb_2Br_5 $\Delta E \sim 620$ cm^{-1} and $\Delta E \sim 650$ cm^{-1} for ETU1 and ETU2, respectively. It should be noted that the energy mismatches is the source of the heat load that accompanies ETU processes [8], which is undesirable, especially at high pump intensities.

The macroscopic upconversion coefficient K_{up} is commonly used to gauge the strength of the energy transfer process, where $K_{up}N$ represents the probability per unit time that an Er^{3+} ion in an intermediate state (N= population density of intermediate state) is elevated to a higher state via upconversion [8,26]. This macroscopic coefficient can be approximated using the following equation [8,26]

$$K_{up} \approx \frac{2\pi C_{DA}}{3R^3} \tag{4}$$

where, C_{DA} is the microparameter for direct energy transfer and R is the minimum Er-Er distance . The minimum Er^{3+} distance is sensitive to Er^{3+} substitution sites and will vary between 4 – 8 Å in KPb_2Cl_5 [3]. The microparameter for energy transfer can be ascertained using Forster-Dexter theory [27,28] for electric dipole-dipole resonant energy transfer shown in equation (5),

$$C_{DX} = \frac{1}{\tau_o} R_{DX}^6 \tag{5}$$

where τ_o is the emission decay time of the donor ion and R_{DX} (X = D for donor or A for acceptor) is the critical radius for direct, resonant energy transfer. The critical radius is defined as the distance between a donor ion and an acceptor ion at which the energy transfer probability is equivalent to the inverse of the inherent emission decay time of the donor. Outside this distance energy transfer cannot take place. This distance can be indirectly measured by utilizing the following equation [27]

$$R_o^6 = \frac{3c\tau_o}{8\pi^4 n^2} \int \sigma_D^{Emis}(\lambda) \cdot \sigma_X^{Abs}(\lambda) d\lambda \tag{6}$$

where, c is the speed of light, n is the index of refraction of the host material, $\sigma_D^{Emis}(\lambda)$ and $\sigma_X^{Abs}(\lambda)$ are the donor's emission and the acceptor's absorption cross-section (or donor's absorption cross-section), respectively. For the case of energy transfer upconversion, where excited ions are elevated to an even higher energy level, $\sigma_X^{Abs}(\lambda)$ is replaced with the excited state absorption cross-section $\sigma_{ESA}^{Abs}(\lambda)$. The excited state absorption cross-section can be easily determined for the infrared upconversion process ($^4I_{13/2} + {}^4I_{13/2} \rightarrow {}^4I_{15/2} + {}^4I_{9/2}$) by employing the Reciprocity relation and converting the 1.7 μm ($^4I_{9/2} \rightarrow {}^4I_{13/2}$) emission cross-section of Er^{3+} to the $^4I_{13/2} \rightarrow {}^4I_{9/2}$ ESA cross-section. The Reciprocity relation is expressed as follows:

$$\sigma_{EM}(\nu) = \sigma_{ABS} \cdot \frac{Z_l}{Z_u} \exp\left[\left(E_{Zl} - h\nu\right)/kT\right] \tag{7}$$

where, σ_{EM} and σ_{ABS} are emission and absorption cross-sections, respectively, E_{ZL} is the energy of the zero phonon line, Z_l and Z_u are the partition functions for the lower and upper states, respectively. Due to the inherently low phonon energy of KPb_2Cl_5 and KPb_2Br_5 the 1.7 μm emission can be easily measured relative to hosts with higher phonon energies such as YAG as nonradiative decay rates are smaller in chloride and bromide based hosts. Using equation (5) the microparameters for the infrared upconversion process ETU1 were determined to be $C_{DA} \sim 3.5 \times 10^{-42}$ cm^6/s and $C_{DA} \sim 2.0 \times 10^{-42}$ cm^6/s for Er: KPb_2Cl_5 and Er: KPb_2Br_5, respectively. A similar infrared upconversion microparameter of $C_{DA} \sim 2.6 \times 10^{-42}$ cm^6/s was reported by Quimby et al.[8] for Er: KPb_2Cl_5. These values are significantly smaller relative to the

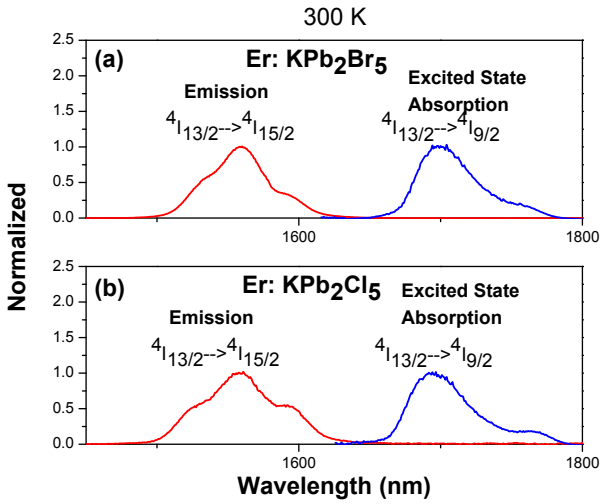

Figure 17. Normalized, room temperature $^4I_{13/2}\rightarrow{}^4I_{15/2}$ emission spectrum and $^4I_{13/2}\rightarrow{}^4I_{9/2}$ excited state absorption spectrum from (a) Er: KPb_2Br_5 and (b) Er: KPb_2Cl_5.

microparameter for Er: YAG which is $C_{DA} \sim 290 \times 10^{-42}$ cm^6/s [8]. The small microparameters is likely an inherent property of the chlorides and bromides because the crystal field at the Er^{3+} site is weaker compared to fluorides and oxides and this results in small overlap integrals between the emission and absorption band [15]. For example, depicted in figures 17a and 17b are the normalized $^4I_{13/2}\rightarrow{}^4I_{15/2}$ emission spectra and $^4I_{13/2}\rightarrow{}^4I_{9/2}$ excited state absorption spectra from Er: KPb_2Br_5 and Er: KPb_2Cl_5, and it is apparent that the small microparameters is evidently due to the very weak coupling between the emission and excited state absorption bands. The ETU microparameter for the green upconversion emission ($^4I_{13/2}$, $^4I_{9/2}$)$\rightarrow$($^4I_{15/2}$,$^2H_{11/2}$ + $^4S_{3/2}$) cannot be easily determined using the above procedure because the $^2H_{11/2}$ + $^4S_{3/2}\rightarrow{}^4I_{9/2}$ emission is strongly coupled to other transitions and the branching ratios are small therefore the $^4I_{9/2}\rightarrow{}^2H_{11/2}$ + $^4S_{3/2}$ ESA cross-section is not easily generated. However, it is anticipated that the ETU2 microparameter is small since the process is nonresonant as well. The critical interaction radii for ETU1was calculated to be $R_{DA} \sim 4.9$ Å and $R_{DA} \sim 3.9$ Å for Er: KPb_2Cl_5 and Er: KPb_2Br_5, respectively. This value is significantly small and is typical for nonresonant energy transfer, for example, nonresonant Tm$\rightarrow$Tm energy transfer ($^3H_4$+$^3H_6\rightarrow{}^3F_4$+$^3F_4$) in $LiYF_4$ crystals yielded a critical interaction radius of approximately ~ 6.0 Å [25]. The small radius implies that excited $^4I_{13/2}$-Er^{3+}ions must be very nearby for direct transfer of energy and therefore direct energy transfer upconversion is less probable. Using the calculated microparameters for the infrared upconversion the macroparameters for ETU1 ranges between $K_{up1} \sim 4.3\times10^{-20}$ - 11.5×10^{-20} cm^3/s and $K_{up1} \sim 0.82\times10^{-20}$ - 5.5×10^{-20} for Er: KPb_2Cl_5 and Er: KPb_2Br_5 (R was approximated as 4 – 8 Å in KPb_2Br_5) , respectively. These values are close to the values reported by Quimby et al. [8], which are 1.06×10^{-20} - 8.5×10^{-20} cm^3/s for Er: KPb_2Cl_5. Interestingly, the upconversion macroparameter for Er: KPb_2Cl_5 and Er: KPb_2Br_5 are two orders of magnitude smaller relative Er: YAG ($K_{up}\sim 25\times10^{-18}$ $cm^3/6$ [8]) indicating that the infrared ($^4I_{13/2}$, $^4I_{13/2}$)$\rightarrow$($^4I_{15/2}$, $^4I_{9/2}$) upconversion process is more aggressive in this host material and therefore more efficiently depopulates the $^4I_{13/2}$, which is undesirable for an efficient 1.5 μm Er^{3+} laser system. Though calculations indicate that infrared upconversion is weak, experimental data illustrates non-negligible upconversion in moderately concentrated samples and consequently it is presumed that the energy transfer between excited $^4I_{13/2}$-Er^{3+} ions is assisted by Er$\rightarrow$Er migration between donors ($^4I_{13/2}$+$^4I_{15/2}$)$\rightarrow$($^4I_{15/2}\rightarrow{}^4I_{13/2}$) until it comes into the neighborhood of an acceptor where energy transfer between two excited $^4I_{13/2}$-Er^{3+} ions can transpire. The critical radius for Er$\rightarrow$Er migration were calculated to be $R_{DD} \sim 16$ Å and $R_{DD} \sim 17$ Å for Er: KPb_2Cl_5 and Er: KPb_2Br_5, respectively, which are quite large but not unexpected due to the small stokes shifts between the $^4I_{13/2}\rightarrow{}^4I_{15/2}$ emission band and $^4I_{15/2}\rightarrow{}^4I_{13/2}$ absorption band of Er^{3+} in KPb_2Cl_5 and KPb_2Br_5 (figures 18a and 18b). Due to the nonresonant nature of the green upconversion it is presumed that this energy

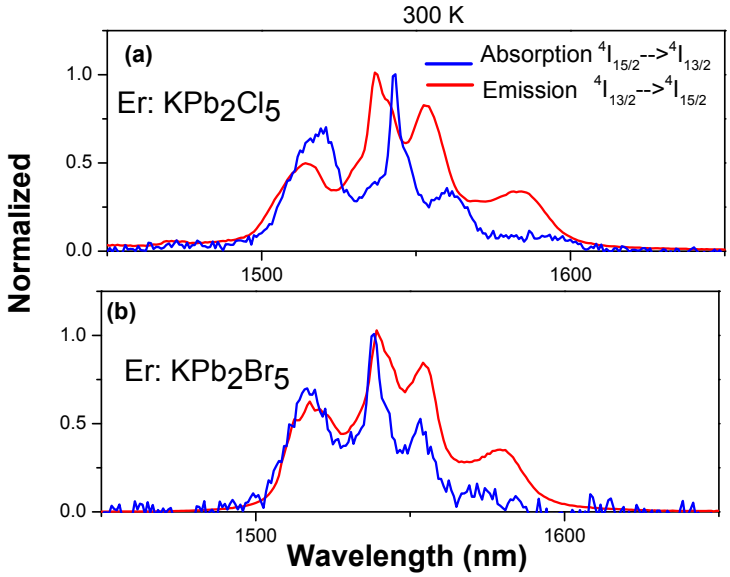

Figure 18. Overlap of room temperature $^4I_{15/2}$→$^4I_{13/2}$ absorption and $^4I_{13/2}$→$^4I_{15/2}$ emission bands from (a) Er: KPb_2Cl_5 and (b) Er: KPb_2Br_5.

transfer process is as well assisted by Er→Er migration.

B. Temperature Dependent Measurements

The dependence of the emission intensities of the upconversion transitions $^2H_{11/2}$ + $^4S_{3/2}$→$^4I_{15/2}$ and $^4I_{9/2}$ →$^4I_{15/2}$ and the $^4I_{13/2}$ →$^4I_{15/2}$ stokes transition on temperature for Er: KPb_2Cl_5 and Er: KPb_2Br_5 are shown in figures 19a – 19d. Similar to room temperature measurements, the samples were excited with ~ 140 mW of 1532 nm laser excitation. The integrated emission intensity were ascertained and it is apparent that the green upconversion in Er: KPb_2Cl_5 does not change significantly between 300 K and 77 K, yet at 10 K the integrated emission intensity is reduced by a factor ~ 0.6 relative to 300 K. Furthermore, at 77 K and 10 K there is negligible population within the $^2H_{11/2}$ given that the band is frozen out which indicate that the $^2H_{11/2}$ and $^4S_{3/2}$ levels are no longer thermally coupled and therefore at low temperature population predominantly resides within the $^4S_{3/2}$. In contrast, the integrated intensity of the green emission from Er: KPb_2Br_5 exhibits significant increase between 300 K – 10 K, where at 10 K the emission

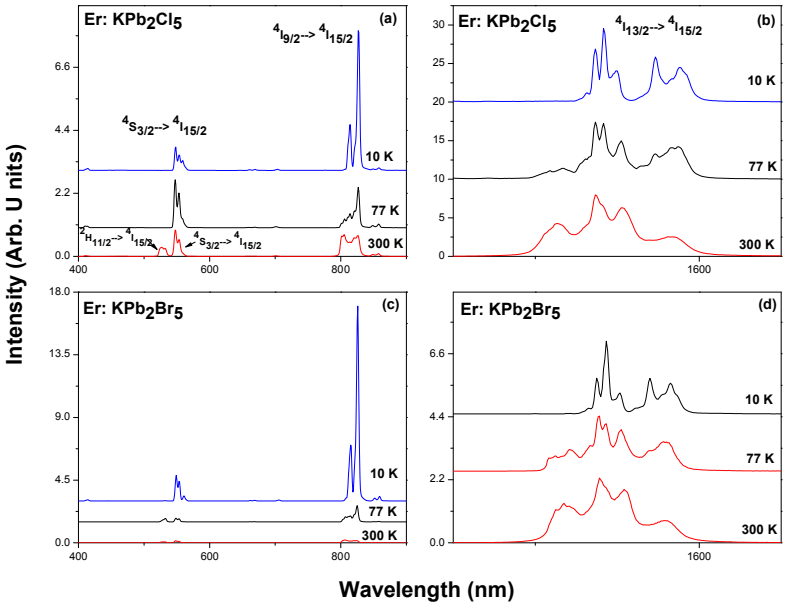

Figure 19. Temperature dependent upconversion emission from (a) Er: KPb_2Cl_5 & (c) Er: KPb_2Br_5 and temperature dependent ~ 1.5 μm emission from emission from (b) Er: KPb_2Cl_5 & (d) Er: KPb_2Br_5.

intensity is a factor of 7 larger relative to 300 K. Interestingly at 77 K, emission from the $^2H_{11/2}$ is still observed in Er: KPb_2Br_5, however at 10 K the $^2H_{11/2}$ is frozen out as well. The $^4I_{9/2} \rightarrow {}^4I_{15/2}$ Infrared upconversion integrated intensity exhibited a moderate increase in Er: KPb_2Cl_5 but there is a more significant rise in Er: KPb_2Br_5. All these results illustrate that upconversion is very active and is not extinguished at lower temperatures and this can be explained by the large donor-donor microparameter at 77K and 10 K, which were calculated to be $C_{DD} \sim 68x10^{-40}$ cm^6/s and $C_{DD} \sim 28x10^{-40}$ cm^6/s for Er: KPb_2Cl_5 and $C_{DD} \sim 153x10^{-40}$ cm^6/s and $C_{DD} \sim 45x10^{-40}$ cm^6/s for Er: KPb_2Br_5, respectively. The large microparameter is not unexpected due to the significant overlap of the $^4I_{13/2} \rightarrow {}^4I_{15/2}$ and $^4I_{15/2} \rightarrow {}^4I_{13/2}$ absorption and emission bands, respectively (figures 20a-20d). It was mentioned earlier that the microparameter (C_{DA}) for direct ETU is small at 300 K and this is due to the weak spectral coupling of the $^4I_{13/2} \rightarrow {}^4I_{15/2}$ emission band and the $^4I_{13/2} \rightarrow {}^4I_{9/2}$ excited state absorption band of the donor ion and acceptor ion, respectively. It is presumed that the spectral coupling should be even less at 77 K and 10 K because narrowing of the absorption and emission bands accompanies low temperature environments. Yet, upconversion persists at low temperatures indicating that donor-donor Er migration is a very efficient mediator for transferring energy to an acceptor at cryogenic temperatures. As the upconversion persist at lower temperatures, the 1.5 μm integrated emission intensity gradually falls between 300 – 10 K. This observation could be due to reduced absorption at the pump wavelength and/or increased efficiency of the two upconversion processes at lower temperatures. According to the low temperature absorption spectra, there is some moderate reductions in the 1532 nm pump absorption between 300 – 10 K for both Er: KPb_2Cl_5 and Er: KPb_2Br_5. However, one would presume a concurrent reduction of the upconversion processes as well. It is apparent that the Er^{3+} system is very complex more exploration is needed to entangle the mechanisms dictating the observed phenomena.

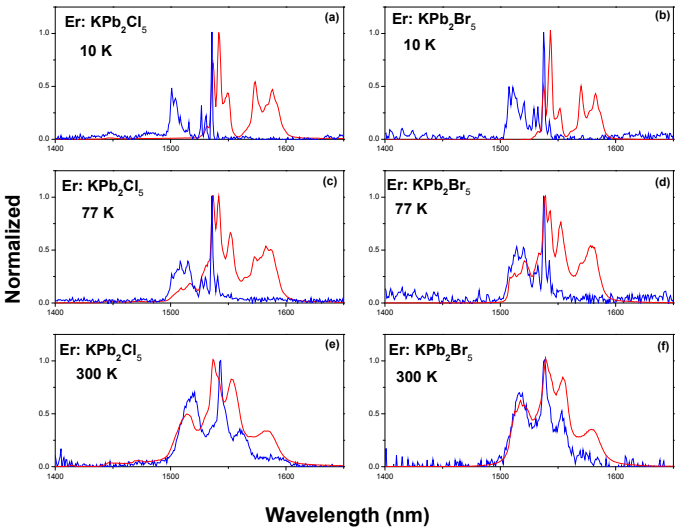

Figure 20. Normalized $^4I_{13/2} \rightarrow {}^4I_{15/2}$ emission spectrum and $^4I_{15/2} \rightarrow {}^4I_{13/2}$ absorption spectrum from Er: KPb_2Cl_5 at (a) 10, (c) 77 K, and (d) 400 K and from Er: KPb_2Br_5 at (b) 10, (d) 77 K, and (f) 400 K.

VIII. Optical Emission and Absorption Spectroscopy of Pr^{3+} Doped in KPb_2Cl_5 and KPb_2Br_5

The emission cross-section spectra of the $^3F_3,{}^3F_4 \rightarrow {}^3H_4$ transition of Pr^{3+} in KPb_2Cl_5 and KPb_2Br_5 was generated by collecting an emission spectrum via ~1440 nm laser diode excitation of $Pr^{3+}$and converting the emission spectrum to emission cross-section using equation (1). Depicted in figure 21 are the emission cross-section spectra originating from the $^3F_3,{}^3F_4 \rightarrow {}^3H_4$ transition of Pr^{3+} in KPb_2Cl_5 and

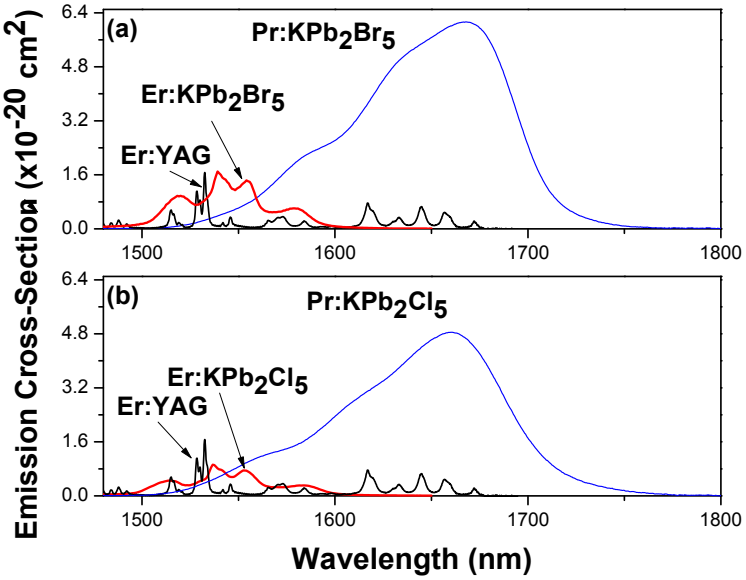

Figure 21 .Room temperature emission cross-section spectra for (a) Pr:KPb_2Br_5, Er: KPb_2Br_5 and Er:YAG (b) Pr:KPb_2Cl_5, Er: KPb_2Cl_5 and Er:YAG.

KPb_2Br_5. As a comparison the emission cross-section of Er^{3+} in the halide hosts KPb_2Cl_5 and KPb_2Br_5 as well as Er: YAG is also included. The peak emission cross-section of Er: KPb_2Cl_5 and Er: KPb_2Br_5 are ~ $0.9x10^{-20}$ cm^2 at 1536 nm and ~ $1.6x10^{-20}$ cm^2 at 1540 nm, respectively, which is slightly smaller compared to Er: YAG (σ_{Emiss}~$1.7x10^{-20}$at 1539 nm). At first glance, it is clear that the emission cross-section spectra arising from Pr^{3+} doped in the halide hosts are broad relative to Er^{3+}possessing a full width at half maximum of ~ 91 nm and 87 nm for Pr: KPb_2Cl_5 and Pr: KPb_2Br_5, respectively. This feature of Pr^{3+} provides a possibility of larger laser tunability in the eye-safe wavelength regime. Moreover, Pr^{3+} has an overall larger peak emission cross-section relative to Er^{3+} doped in the halide hosts as well as the more traditional host YAG. The peak emission cross-section of Pr: KPb_2Cl_5 and Pr: KPb_2Br_5 are $4.8x10^{-20}$ cm^2 at 1661 nm and $6.1x10^{-20}$ cm^2 at 1667 nm, respectively. It is common knowledge that Pr^{3+} is a promising ion because it has one of the largest emission cross-sections amongst rare-earth ions for many laser transitions. For example, a large $^3F_3$,$^3F_4 \rightarrow {}^3H_4$ emission cross-section from Pr: $RbPb_2Cl_5$ was reported by Okhrimchuk et al. [29] having a large peak value of approximately $1.0x10^{-19}$ cm^2. Further, lasing originating from the $^3F_3$,$^3F_4 \rightarrow {}^3H_4$ transition of Pr^{3+} was demonstrated by Dubinski et al. [20] at cryogeneic temperature.

Temporal emission measurements corresponding to the $^3F_3$,$^3F_4 \rightarrow {}^3H_4$ transition of Pr^{3+}in KPb_2Cl_5 and KPb_2Br_5 are shown in figure 22. For comparison, the $^4I_{13/2} \rightarrow {}^4I_{15/2}$ transition of Er^{3+} in KPb_2Cl_5 is included. Due to some samples possessing nonlinear decay characteristics all the emission decay times were calculated using the following equation [30],

$$\tau = \frac{1}{I_o}\int_0^\infty I(t)dt \qquad (8)$$

where I(t) is the emission intensity as a function of time and I_o is the emission intensity at t = 0 s. The samples containing Pr^{3+} as a dopant were excited at ~1436 nm using a Nd: YAG pumped OPO system and the emission was monitored at 1630 nm. The samples containing Er^{3+} were excited with the same OPO system but the laser was tuned to 1505 nm and emission was monitored broad-band while coupled with a band-pass filter. The temporal emission measurements corresponding to the $^3F_3$,$^3F_4 \rightarrow {}^3H_4$ transition of two samples (labeled sample 1 and sample 2) of Pr: KPb_2Br_5 are shown in figure 22b. The emission decay of the weaker concentrated sample (Sample 1;N=$7.1x10^{18}$ cm^{-3}) appears to not be quenched yielding a linear decay transient with a decay time of ~ 537 μs whereas sample 2 has a concentration of about an order of magnitude larger (N=$7.6x10^{19}$ cm^{-3}) which resulted in a nonlinear decay and a reduced

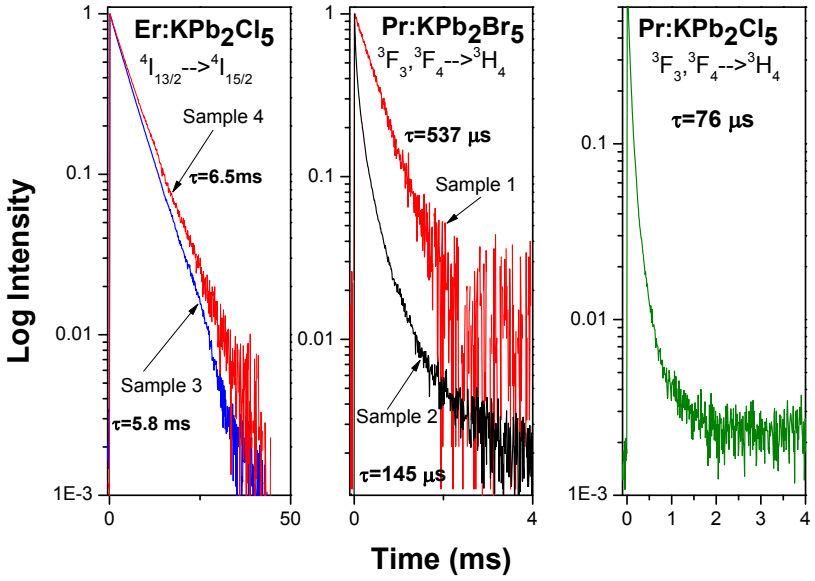

Figure 22. Emission decay transients from (a) two concentrations of Er: KPb_2Cl_5, (b) two concentrations of Pr: KPb_2Br_5 and (c) Pr: KPb_2Cl_5.

decay time of ~ 145 μs. According to Judd-Ofelt analysis the radiative decay of the $^3F_3,^3F_4 \rightarrow ^3H_4$ transition of Pr: KPb_2Br_5 [31] is ~0.3 ms which is shorter than the ~ 0.5 ms measured decay time of the weakest concentrated sample (sample 1). The longer decay time could indicate that radiation trapping is lengthening the emission decay time as it is well known that significant overlap of absorption ($^3H_4 \rightarrow ^3F_3,^3F_4$) and emission ($^3F_3,^3F_4 \rightarrow ^3H_4$) bands can lead to the radiation trapping effect [32]. The shorter and nonlinear decay of sample 2 is likely attributed to cross-relaxation and upconversion processes which quenches the $^3F_3,^3F_4$ level. In addition, due to the close proximity of the $^3F_3,^3F_4$ and $^3F_2,^3H_6$ coupled levels some multi-phonon decay to the $^3F_2,^3H_6$ level could also contribute to the quenching of the $^3F_3,^3F_4$ level. However, multiphonon quenching is expected to be less severe in the low phonon energy hosts KPb_2Cl_5 and KPb_2Br_5. Similar nonlinear decay characteristics were reported by Ferrier et al. [33] in Pr: KPb_2Cl_5 and Pr: $CsCdBr_5$ under 1.54 μm laser excitation and the nonexponential decay behavior was proposed to be due to the following cross-relaxation processes: $(^3F_3+^3H_4) \rightarrow (^3F_2+^3H_5)$ and $(^3F_3+^3H_5) \rightarrow (^3F_2+^3F_2)$ [18, 31]. Cross relaxation appears to not contribute significantly to the decay dynamics of sample 1 because this process becomes more active at larger dopant concentrations. Figure 22c depicts the emission decay transient of the $^3F_3,^3F_4 \rightarrow ^3H_4$ transition of Pr: KPb_2Cl_5 and comparable to Pr: KPb_2Br_5 there is quenching of this level with an even shorter decay time of ~76 μs. The emission decay of the $^4I_{13/2} \rightarrow ^4I_{15/2}$ transition of two samples (labeled sample 1 and sample 2) of Er: KPb_2Cl_5 are shown in figure 22a. It is apparent that Er^{3+} emission decay is linear and has an intrinsically longer decay time of ~5.8 ms (sample 3) and 6.5 ms (sample 4) compared to Pr^{3+} doped in the halide hosts whose decay times are in the μs time regime. The inherently longer emission decay time of Er^{3+} relative to Pr^{3+} is attributed to its smaller emission cross-section in KPb_2Cl_5, which is an attractive feature for efficient energy storage. However, long emission decay times can enhance the probability for higher-order upconversion processes which is a problem for 1.5 μm pumped Er-doped laser materials. Judd-Ofelt analysis indicates that the radiative decay time of the $^4I_{13/2} \rightarrow ^4I_{15/2}$ transition of Er: KPb_2Cl_5 is ~4.2 ms [24] which is shorter than the measured decay times of samples 3 and 4. The longer decay time of Er: KPb_2Cl_5 is attributed to radiation trapping which is common for the $^4I_{13/2} \rightarrow ^4I_{15/2}$ transition of Er^{3+}. Though radiation trapping increases the emission decay time of the $^4I_{13/2} \rightarrow ^4I_{15/2}$ transition of Er^{3+}, upconversion is present which also contributes to the effective decay transient. Similar to Pr^{3+} in the halide hosts KPb_2Cl_5 and

KPb_2Br_5 nonradiative decay through multiphonon-emission should also be weak for the $^4I_{13/2} \rightarrow {}^4I_{15/2}$ transition of Er^{3+}.

Visible emission was generated by exciting Pr^{3+} with a Nd: YAG pumped OPO tuned to ~ 474 nm and ~ 590 nm (5 ns pulses, 10 Hz). Figure 23 shows the emission spectra of Pr: KPb_2Cl_5 and Pr: KPb_2Br_5 after laser excitation of the $^3P_1$ (474 nm) and $^1D_2$ (590 nm) absorption bands. Following 474 nm laser excitation the spectrum consists of lines originating from the $^3P_0 \rightarrow {}^3H_4, {}^3H_5, {}^3H_6, {}^3P_0 \rightarrow {}^3F_2$, $^3P_1 \rightarrow {}^3H_5, {}^3H_6$ and $^3P_1 \rightarrow {}^3F_2$, $^3F_{3,4}$ transitions. The most intense emission from Pr: KPb_2Cl_5 is red (~648 nm) corresponding to the $^3P_0 \rightarrow {}^3F_2$ transition, whereas Pr: KPb_2Br_5 most dominant emission is green (~532 nm) corresponding to the $^3P_1 \rightarrow {}^3H_5$ transition. Following 590 nm excitation a strong red line at ~615 nm and a weaker red line at ~670 nm corresponding to $^1D_2 \rightarrow {}^3H_4$ and $^1D_2 \rightarrow {}^3H_5$ transitions, respectively, were observed. The emission decay arising from the $^3P_0 \rightarrow {}^3F_2$, $^3P_1 \rightarrow {}^3H_5$ and $^1D_2 \rightarrow {}^3H_5$ transitions were explored in Pr: $KPb_2Cl_5$and Pr: KPb_2Br_5.The decay transients were obtained by exciting the $^3P_1$ and $^1D_2$ bands of Pr^{3+} and the emission was monitored at 650 nm ($^3P_0 \rightarrow {}^3F_2$), 532 nm ($^3P_1 \rightarrow {}^3H_5$) and 620 nm ($^1D_2 \rightarrow {}^3H_5$). Figures 24a and 24c depicts the $^3P_1 \rightarrow {}^3H_5$ emission decay transients from Pr:$KPb_2Cl_5$and Pr: KPb_2Br_5,

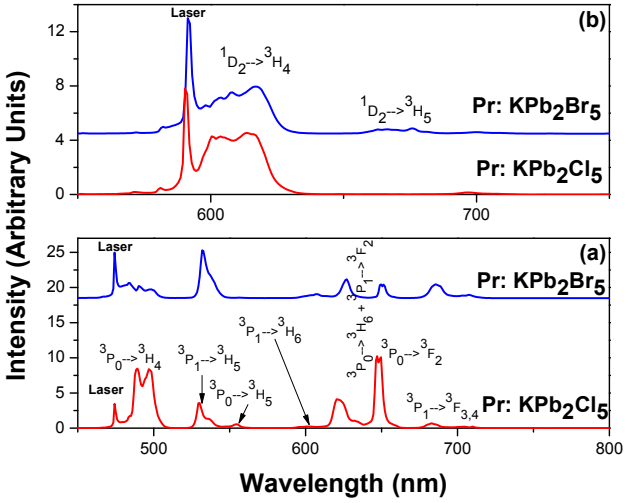

Figure 23. Visible emission obtained by exciting Pr: $KPb_2Cl_5$and Pr: KPb_2Br_5at (a) 474 nm and (b) 590 nm (Note: the 590 nm and 474 nm laser wavelengths are coupled with the $^1D_2 \rightarrow {}^3H_4$ emission and $^3P_0 \rightarrow {}^3H_4$ emission, respectively.)

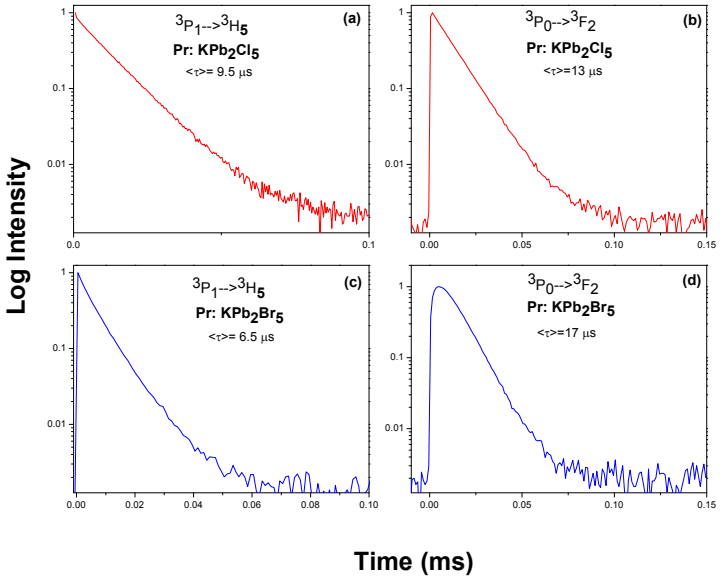

Figure 24. Visible emission decay transients from Pr: KPb_2Cl_5 arising from the (a)$^3P_1 \rightarrow {}^3H_5$and(b) $^3P_0 \rightarrow {}^3F_2$transition. Visible emission decay transients from Pr: KPb_2Br_5 arising from the (c)$^3P_1 \rightarrow {}^3H_5$and(d) $^3P_0 \rightarrow {}^3F_2$transitions.

respectively. The emission decays are linear with a decay time of ~9.5 μs and ~6.5 μs for Pr: KPb_2Cl_5 and Pr: KPb_2Br_5, respectively. The measured emission decay time of Pr: KPb_2Cl_5 is similar to the results reported by Balda et al [34] their value was 11.3 μs. Since the emission from the $^3P_0$ level was generated by populating the $^3P_1$ level initially the $^3P_0 \rightarrow {}^3F_2$ decay transients shows some rise time indicating that the $^3P_1$ is relaxing to the $^3P_0$ level (figures 24b and 24d). The emission decay times of the $^3P_0 \rightarrow {}^3F_2$ transition are 13 μs and 17 μs for Pr: KPb_2Cl_5 and Pr: KPb_2Br_5, respectively. Following 590 nm laser excitation of the $^1D_2$ absorption band of Pr^{3+} emission decay transients corresponding to the $^1D_2 \rightarrow {}^3H_5$ transition from Pr: KPb_2Cl_5 and Pr: KPb_2Br_5 were collected and is shown in figure 25. The emission decay transients of the $^1D_2 \rightarrow {}^3H_5$ transition are nearly linear with a decay time of 25 μs and 22 μs for Pr: KPb_2Cl_5 and

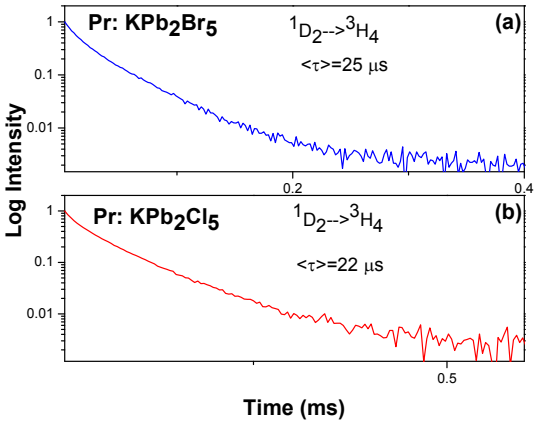

Figure 25. Visible emission decay transients corresponding to $^1D_2 \rightarrow {}^3H_5$ transition arising from (a)Pr: KPb_2Br_5 and(b) Pr: KPb_2Cl_5.

Pr: KPb_2Br_5, respectively. Interestingly, the emission decay time of the $^1D_2 \rightarrow {}^3H_5$ transition of Pr: KPb_2Cl_5 is significantly shorter compared to 70 µs decay time reported by Balda et al. [34].

Very little work has been reported on the upconvesion emission following excitation of the $^3F_3$,$^3F_2$ band of Pr^{3+}which however needs to be understood as this process could significantly contribute to the dynamics of a potential resonantly pumped Pr-system. As recently discussed, resonant pumping of the $^3F_3$,$^3F_4$ band of Pr^{3+}yields broad infrared emission in the 1500-1750 nm range, unfortunately, upconversion emission accompanies this pump scheme which reduces the overall pump efficiency and in addition deposits unwanted heat into the crystal. Displayed in figure 26a are the visible upconversion emission spectra from Pr: KPb_2Br_5 excited with a Nd: YAG pumped OPO operating at ~1550 nm (5 ns pulses, 10 Hz). As a comparison the visible emission stimulated by 474 nm and 590 nm laser excitation is also included in figure 26a. Similar to exciting Pr^{3+} at 474 nm (figure 23a) emission from the $^3P_0 \rightarrow {}^3H_4$,$^3H_6$,$^3F_2$ and $^3P_1 \rightarrow {}^3H_5$, $^3F_2$, $^3F_{3,4}$ transitions were observed. Upconversion emission arising from

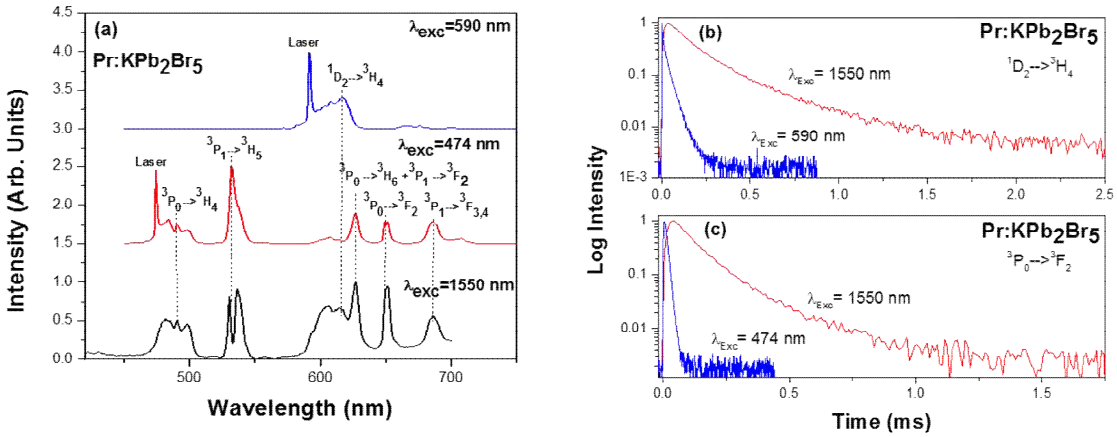

Figure 26. (a) Visible emission from Pr: KPb_2Br_5 via 550 nm, 474 nm, and 590 nm pulsed laser excitation. (b) Visible emission decay transients from the $^1D_2$ state under 1550 nm and 590 nm excitation and (c) Visible emission decay transients from the $^3P_0$ state under 1550 nm and 590 nm excitation.

from the $^1G_4 \rightarrow {}^3H_4$ transition was not measured in this study but was observed by Okhrimchuk et al. [35] under excitation of the $^3F_3$,$^3F_4$ band of Pr: $RbPb_2Cl_5$. An additional emission band not seen under 474 nm excitation corresponding to the $^1D_2 \rightarrow {}^3H_4$ transition was observed and can be also be generated directly by exciting the $^1D_2$ absorption band of Pr^{3+}(figure 23b). According to reference [36] the visible upconversion in a similar system, Pr: $Rb_2Pb_2Cl_5$, is suggested to be attributed to the following scheme: (1) upconversion to the $^1G_4$ level via this process $^3F_3 + {}^3F_3 \rightarrow {}^1G_4 + {}^3H_5$ which contributes to the $^3H_5$ population and (2) a series of excited state absorption (ESA) of the pump which leads to populating the $^1D_2$ and $^3P_{1,2,3}$ states via the following processes: Pump + $^3H_5 \rightarrow {}^1G_4$, Pump + $^1G_4 \rightarrow {}^1D_2$ and Pump + $^1D_2 \rightarrow {}^3P_{1,2,3}$. However in Pr: KPb_2Br_5 the decay transients of the emission coming from the $^1D_2$ state (600 nm) and $^3P_0$ states (650 nm) suggests that energy transfer upconversion (ETU) is responsible for populating the visible emitting states under 1.5 µm excitiation. The transients show a significant rise time after the laser pulse followed by a decay timeof $\tau \sim 213$ µs and $\tau \sim 140$µs for the $^1D_2$ and $^3P_0$ states, respectively (figure 26). The emission decay times are significantly longer relative to direct excitation of the $^1D_2$ ($\tau \sim 25$ µs) and $^3P_0$($\tau \sim 17$µs) states. This feature is indicative of nonradiative ETU process taking place. Now, to obtain population within the $^1D_2$ and $^3P_{0,1}$ levels, the $^1G_4$ level must be populated. Initially, the 1.5 µm pump populates the $^3F_3$,$^3F_2$ levels and due to the resonance conditions amongst the $^3F_3 \rightarrow {}^3H_5$ and $^3F_3 \rightarrow {}^1G_4$ transitions the following ETU process is possible $^3F_3 + {}^3F_3 \rightarrow {}^3H_5 + {}^1G_4$ [figure 27a; 33] which provides a channel for populating the $^1G_4$. Once there is population within the $^1G_4$ state the $^1D_2$ state is populated through the ETU process $^1G_4 + {}^1G_4 \rightarrow {}^1D_2 + {}^3H_5$ [figure 27b; 37]. Finally, once there is concurrent population within the

$^1G_4$ and $^1D_2$ levels the $^3P_0$ and $^3P_1$ levels may be populated via this ETU channel $^1G_4+^1D_2 \rightarrow ^3H_5+^3P_1$ [figure 27c; 37]. In addition, if there is significant population in the $^3F_2$ level the $^3P_0$ level could be populated via this ETU process $^1D_2+^3F_2 \rightarrow ^3P_0+^3H_4$ [figure 27d; 37].

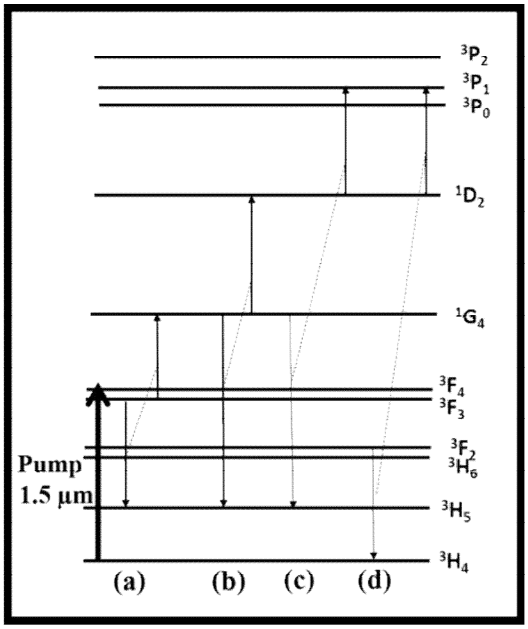

Figure 27. Schematic energy level diagram of Pr^{3+}. (a) ETU process $^3F_3+^3F_3 \rightarrow ^3H_5+^1G_4$, (b) ETU process $^1G_4+^1G_4 \rightarrow ^1D_2+^3H_5$, (c) ETU process $^1G_4+^1D_2 \rightarrow ^3H_6+^3P_1$and (d) ETU process $^1G_4+^1D_2 \rightarrow ^3H_6+^3P_1$.

Though Pr^{3+} upconversion was observed under resonant pumping of the $^3F_3$,$^3F_4$ absorption band the magnitude of this process appears to be weaker relative to the upconversion emission observed in Er^{3+} doped materials such as YAG under resonant pumping of the $^4I_{13/2}$ absorption band. Similar observation was reported by Dubinskii et al. [20] in Pr: $RbPb_2Cl_5$ where upconversion also appears to be less severe compared to the resonant pumped Er-systems. In Pr:$RbPb_2Cl_5$ orange upconversion emission under 1.45 μm excitation is only visibly observed if the laser beam is focused very tightly [29]. However, the upconversion emission was not observed with a larger diameter pump beam which indicates that the sample has to be pumped very hard in order to achieve significant upconversion. Shown in figure 28 are the upconversion emission visibly observed with the naked eye from Er: KPb_2Cl_5 and Pr:KPb_2Br_5 excited at ~1532 nm by employing an Er-Fiber laser operating at ~ 1.0 Watts. Clearly, the green emission arising from Er^{3+} is strong even when the ceiling lights are on (figure 28a). On the other hand, the reddish light emitted by Pr^{3+} is only clearly observable in the dark (figure 28c). Figure 28b shows the Pr:KPb_2Br_5 sample under 1532 nm laser excitation with the ceiling lights on where the visible upconversion is not clearly observed.

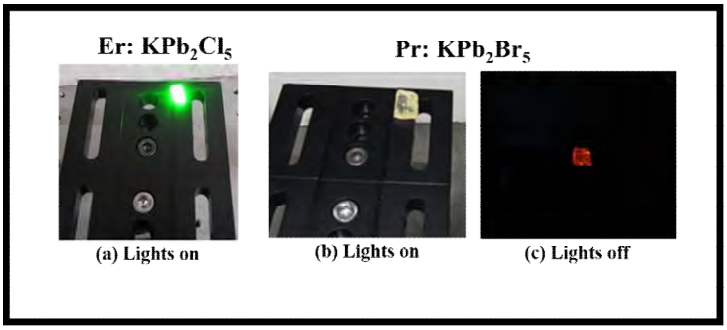

Figure 28. Upconversion emission photographed after 1532 nm cw laser excitation of (a) Er: KPb_2Cl_5 with lightson, (b) Pr: KPb_2Br_5 with lights on and (c)Pr: KPb_2Br_5 with lights off.

IX. Infrared (1.5-1.6 µm) Gain Cross-Section for Pr^{3+} and Er^{3+}

To obtain an impression on the laser performance of the investigated rare-earth ions the gain cross-section of the $^3F_3, ^3F_4 \rightarrow ^3H_4$ and $^4I_{13/2} \rightarrow ^4I_{15/2}$ transitions of Pr^{3+} and Er^{3+}, respectively were calculated. The absorption and emission cross-sections were utilized for ascertaining the laser gain cross-sections according to the equation [38]:

$$G(\lambda) = \beta\sigma_{emiss}(\lambda) - (1-\beta)\sigma_{abss}(\lambda) \quad (2)$$

where, β is the population inversion ratio, σ_{Emiss} and σ_{Abs} are the emission and absorption cross-sections, respectively. Figure 29 displays the gain cross-sections for various inversion ratios (β = 0, 0.25, 0.5, 0.75, and 1) for Er: KPb_2Cl_5, Er: $KPb_2Br_5$and Er: YAG. In addition, figure 30 depicts the gain cross-sections for Pr: KPb_2Cl_5 and Pr: KPb_2Br_5 as a function of the inversion ratio β as well. The gain cross-section for Er^{3+} in the bromide hosts presents larger gain relative to the chloride host. For example, the peak gain cross-section for a population inversion ratio of β=0.75 are ~ $0.47\text{x}10^{-20}$ cm^2 at 1553 nm and ~ $0.87\text{x}10^{-20}$ cm^2 at 1555 nm, for Er: KPb_2Cl_5 and Er: KPb_2Br_5, respectively. On the other hand, Er: YAG

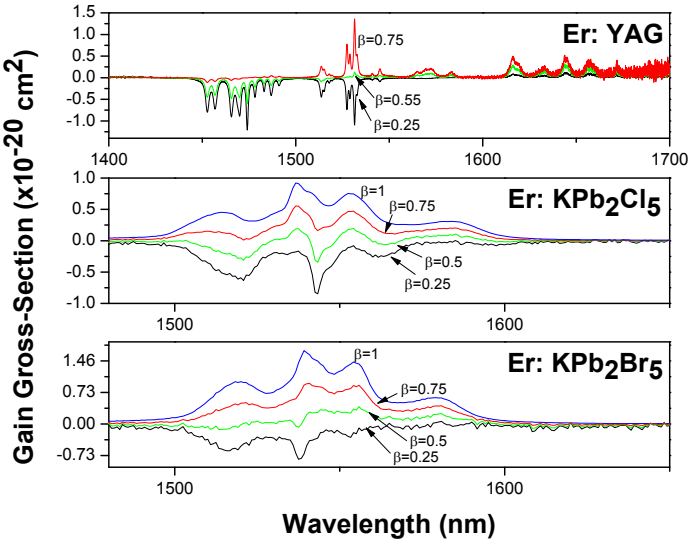

Figure 29. Gain cross-section of the $^4I_{13/2} \rightarrow ^4I_{15/2}$ laser transition of $Er^{3+}$for (a) Er: $KPb_2Cl_5$and (b)Er: $KPb_2Br_5$and (c) Er: YAG for different inversion ratios β.

possesses the largest peak gain cross-section of ~ $1.3\text{x}10^{-20}$ cm^2 at 1531 nm relative to Er^{3+} in either halide hosts. Similar to Er^{3+}, the gain cross-section of Pr^{3+} is also larger in the bromide host relative to the

chloride host. As recently discussed, Pr^{3+} possesses an overall larger absorption and emission cross-sections relative to Er^{3+}in the halide and YAG hosts. Thus, it is not surprising that Pr^{3+} has a larger gain cross-section suggesting that smaller laser power threshold is required for stimulated emission and therefore more efficient pumping conditions is anticipated. For example, the peak gain cross-section for a population inversion ratio of β=0.75 are ~ $3.5x10^{-20}$ cm^2 at 1663 nm and ~ $4.4x10^{-20}$ cm^2 at 1669 nm, for Pr: KPb_2Cl_5 and Pr: KPb_2Br_5, respectively. Moreover, the gain cross-section for Pr: KPb_2Cl_5 and Pr: KPb_2Br_5 is positive between ~ 1570-1755 nm providing a possibility of wide range of laser tunability at longer wavelengths in the eye-safe wavelength regime.

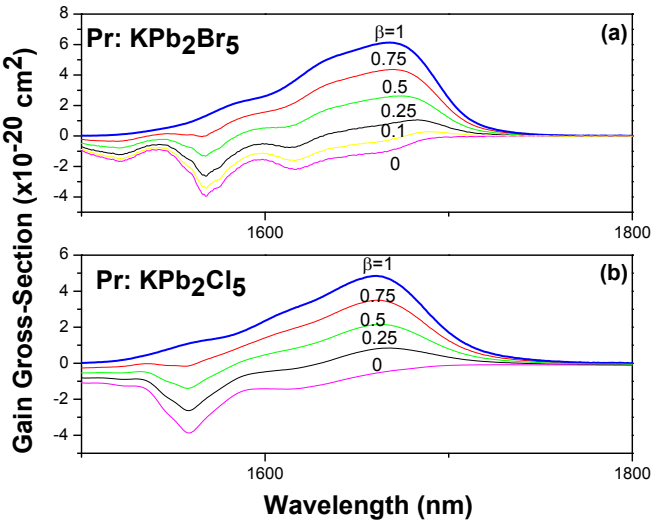

Figure 30. Gain cross-section of the $^3F_4,^3F_3 \rightarrow {}^3H_4$ laser transition of $Pr^{3+}$for (a) Pr: $KPb_2Cl_5$and (b)Pr: $KPb_2Br_5$for different inversion ratios β.

X. Conclusion

Crystal growth along with spectroscopic studies were conducted on Er^{3+} and Pr^{3+} doped in KPb_2Cl_5 and Er: KPb_2Br_5. For a comparison some of the results were related to the extensively investigated Er: YAG system. The significant difference in the spectroscopic properties of Pr^{3+}relative Er^{3+} in the halide hosts are its superior absorption ($^3H_4 \rightarrow {}^3F_3,^3F_4$), emission ($^3F_3,^3F_4 \rightarrow {}^3H_4$) and effective gain ($^3F_3,^3F_4 \rightarrow {}^3H_4$) cross-sections. These results are not surprising for Pr^{3+} in general has one of the largest emission cross-sections amongst rare-earth ions for many laser transitions. Measurements show that the peak absorption cross-sections of Pr: KPb_2Cl_5 and Pr: KPb_2Br_5 are ~ $3.4x10^{-20}$ cm^2 and $3.5x10^{-20}$ cm^2 , respectively, which are nearly a factor of two larger than the $^4I_{13/2} \rightarrow {}^4I_{15/2}$ absorption cross-section of Er^{3+}doped in KPb_2Cl_5 and KPb_2Br_5. Further, the peak absorption cross-section of Pr^{3+} also surpasses the ~ $2.4x10^{-20}$ cm^2 $^4I_{13/2} \rightarrow {}^4I_{15/2}$ absorption cross-section of Er:YAG. Similar results were also observed in the emission cross-sections of Pr^{3+}. The peak emission cross-sections for Pr: KPb_2Cl_5 and Pr: KPb_2Br_5 are ~ $4.8x10^{-20}$ cm^2 and ~ $6.1x10^{-20}$ cm^2, respectively, whereas the peak emission cross-sections of Er: KPb_2Cl_5, Er: KPb_2Br_5 and Er: YAG are ~ $0.9x10^{-20}$ cm^2,~ $1.6x10^{-20}$ cm^2 and $1.7x10^{-20}$ cm^2, respectively. Moreover, emission cross-section spectra arising from $Pr^{3+}$are broad relative to Er^{3+}providing an opportunity for larger laser tunability in the eye-safe wavelength regime. The effective gain cross-section of Pr^{3+} is very attractive for an eye-safe laser extended to wavelengths beyond 1600 nm, which is not possible for Er^{3+}. The gain cross-sections (β=0.75) for Pr: KPb_2Cl_5 and Pr: KPb_2Br_5 are positive between ~ 1570-1755 nm providing a possibility of wide range of laser tunability. In addition, the magnitude of the gain cross-sections for Pr^{3+} is significantly

larger relative to Er^{3+}. For example, the peak gain cross-section for a population inversion ratio of β=0.75 are ~ $3.5x10^{-20}$ cm^2 at 1663 nm and ~ $4.4x10^{-20}$ cm^2 at 1669 nm, for Pr: KPb_2Cl_5 and Pr: KPb_2Br_5, respectively, while the peak gain cross-sections for a population inversion ratio of β=0.75 are ~ $0.47x10^{-20}$ cm^2 at 1553 nm, ~ $0.87x10^{-20}$ cm^2 at 1555 nm, and ~ $1.3x10^{-20}$ cm^2 at 1531 nm for Er: KPb_2Cl_5, Er: KPb_2Br_5, and Er: YAG, respectively. Our experimental results indicate that ETU was occurring under resonant pumping of the $^4I_{13/2}$ and $^3F_3$,$^3F_4$ bands Er^{3+} and Pr^{3+}, respectively. Exciting the $^3F_3$,$^3F_4$ band of Pr^{3+}provides a channel for visible upconversion which accompanies the 1.5-1.6 μm infrared emission and therefore removes population from the $^3F_3$,$^3F_4$ level and direct population into the higher lying $^3P_0$,$^3P_1$, and $^1D_2$ states. However an additional dynamical process namely cross-relaxation could also contributes to the depopulation of the $^3F_3$,$^3F_4$ level of Pr^{3+}which indicates that lower Pr^{3+}concentration is necessary in order to reduce the activation of these processes. It was observed that $^4I_{9/2}\rightarrow{}^4I_{15/2}$ infrared upconversion and the $^2H_{11/2}$ + $^4S_{3/2}\rightarrow{}^4I_{15/2}$ green upconversion are the most dominant upconversion channels in Er: KPb_2Cl_5 and Er: KPb_2Br_5. Using calibrated emission data the relative populations (N_{545nm}/N_{IR} nm) between the $^2H_{11/2}$ + $^4S_{3/2}$ and $^4I_{9/2}$ levels were determined to be ~ 0.04 and ~ 0.02 for Er: KPb_2Cl_5 and Er: KPb_2Br_5, respectively. The excitation spectra along with the emission decay transients of the infrared and green upconversion were collected and strongly suggests that ETU is the mechanism responsible for the $^4I_{9/2}\rightarrow{}^4I_{15/2}$ and $^2H_{11/2}$ + $^4S_{3/2}\rightarrow{}^4I_{15/2}$ upconversion emissions in Er: KPb_2Cl_5 and Er: KPb_2Br_5. The upconversion microparameters for the infrared upconversion are very small having the values C_{DA} ~ $3.5x10^{-42}$ cm^6/s and C_{DA} ~ $2.0x10^{-42}$ cm^6/s for Er: KPb_2Cl_5 and Er: KPb_2Br_5, respectively. Due to the strong spectral overlap of the $^4I_{13/2}\rightarrow{}^4I_{15/2}$ emission and $^4I_{15/2}\rightarrow{}^4I_{13/2}$ absorption bands Er-Er migration is beleived to be assisting the energy transfer upconversion process in both Er: KPb_2Cl_5 and Er: KPb_2Br_5. Calculations indicate that the probability for energy migration is large yielding donor-donor microparameters of C_{DA} ~ $4.3x10^{-39}$ cm^6/s and C_{DA} ~ $1.3x10^{-38}$ cm^6/s for Er: KPb_2Cl_5 and Er: KPb_2Br_5, respectively. Strong 1550 nm infrared emission was observed from both Er: KPb_2Cl_5 and Er: KPb_2Br_5. The relative populations (N_{810nm}/N_{1500} nm) between the $^4I_{9/2}$ and $^4I_{13/2}$ levels were determined to be ~ 0.001 and ~ 0.0005 for Er: KPb_2Cl_5 and Er: KPb_2Br_5, respectively, suggesting significantly larger population within the $^4I_{13/2}$ relative to the $^4I_{9/2}$ and $^2H_{11/2}$ + $^4S_{3/2}$ levels. At lower temperature upconversion remains active and is tentatively attributed to efficient Er-Er migration at cryogenic temperatures.

XI. REFERENCES

[1] Ter-Gabrielyan, N., Merkle, L. D. , Ikesue, A. and Dubinskii, M.,"Ultra low quantum defect eye-safe Er:Sc_2O_3 Laser," Opt. Lett. 33(13), 1524-1526 (2008).

[2] Merkle, L. D., Ter-Gabrielyan, N., Dubinskii, M. and Ikesue, A.,"Cross sections for room and low temperature operation of Er-doped Sesquioxide lasers,"CLEO in Tech. Dig. ChDD1, OSA (2007).

[3] Young, Y. E., Setzler, S. D. , Snell, K. J., Budni, P. A., Pollak, T. M. and Chocklis, E. P., Optics Letters, "Efficient 1645 nm Er:YAG laser," 29, 1075-1077 (2004).

[4] Chang, N. W.H. , Simakov, N., Hosken, D. J., Munch, J., Ottaway, D. J. and Veitch, P. J., "Resonantly diode-pumped continuous-wave and Q-swithched Er:YAG laser at 1645 nm,"Opt. Exp. 18, 1367-13678 (2010).

[5] Ter-Gabrielyan, N., Fromzel,V., Lukasiewicz, T,Ryba-Romanowski, W. and Dubinskii, M., "Nearly quantum defect limited efficiency, resonantly pumped, Er^{3+}:YVO_4 laser at 1593.5 nm," Opt. Lett. 36, 1218-1220 (2011).

[6] Setzler, S. D., Francis, M. P., Young, Y. E., Konves, J. R. and Chicklis, E. P., "Resonantly pumped eyesafe erbium lasers,", IEEE J. Se.Top Quantum Electron. 11, 645 (2005).

[7] White, J. O., Dubinskii, M., Merckle, L. D., Kudryashov, I. and Garbuzov, 'Resonantly pumping and upconversion in 1.6 μm Er^{3+} Lasers," J. Opt. soc.Am. B 24, 2454 (2007).

[8] Quimby, R. S., Condon, N. J., O'Connor, S. P., Biswal, S., and Bowman,S. R.,"Upconversion an excited state absorption in the lower levels of Er: KPb_2Cl_5,"Opt Mater.30, 827-834 (2008).

[9] Dubinskii, M., Ter-Gabrielyan, N., Camargo, M.,Newburgh, G. A. and Merkle, L. D., "Ultra-Low-Photon-Defect Cryo-Laser Performance of Resonantly Diode-Pumped Er^{3+}:YAG," CLEO in Tech. Dig. CTuN1, OSA (2007).

[10] Rieder, T. and Güdel,H. U., "Upconversion dynamics of Er^{3+}doped $RbGd_2Br_7$," J. Chem. Phys. 107, 2169-2174 (1997).

[11] Balda, R., Garcia-Adeva,A. J.,Voda, M. and Fernandez,J., "Upconversion processes in Er^{3+} doped KPb_2Cl_5, Phys. Rev.B," 69, 205203-1 – 205203-8 (2004).

[12] Hömmerich,U., Nyein, E. E. and Trivedi, S. B., "Crystal growth, upconversion and infrared emission properties of Er^{3+} doped KPb_2Br_5", J. Lumin. 113, 100-108 (2005).

[13] Garcia-Adeva, A. Balda, J. R., Fernandez, J., Nyein,E. E. and Hömmerich, U., "Dynamics of the infrared-to-visible upconversion in an Er^{3+} doped KPb_2Br_5crystal," Phys. Rev. B, 72 165116-1 – 165116-11 (2005).

[14] Tkachuk,A. M., Ivanova, S. E.,Joubert, M. F., Guyot, Y., Isaenko, L. I. and Gapontsev,V. P., "Upconversion processes in Er^{3+}: KPb_2Cl_5laser crystals," J. Lumin. 125, 271-278 (2007).

[15] Ferrier, A.,Velazquez,M., Doualan,J. L. and Moncorge, R., "Energy level and excited state absorption properties of Er^{3+} doped KPb_2Cl_5," J. Opt. Soc. Am. B 9, 2526-2536 (2007).

[16] Lüthi, S. R., Pollnau, M. and Güdel, H. U., "Near-infrared to visible upconversion in Er^{3+}-doped $Cs_3Lu_2Cl_9$, $Cs_3Lu_2Br_9$, and $Cs_3Lu_2I_9$excited at 1.54 μm," Phys. Rev. B 60, 162-178 (1999).

[17] S. R. Bowman, N., Merkle, L. B. Shaw, B. J. Feldman, and J. Ganem," IEEE Journal of Quantum Electronics 32 (1996)646.

[18] S. M. Kirkpatrick, S. R. Bowman, and L. B. Shaw, J. Appl. Phys. 82 (1997) 2759.

[19] A. G. Okhrimchuk, L. N. Butvina, E. M. Dianov, N. V. Lichkova, V. N. Zagorodnev, and A. V. Shestakov 36 (2006) 41.

[20] M. Dubinskii, N. Ter-Gabrielyan, M. Camargo, G. A. Newburgh, and L. D. Merkle, in 2007 Conference on Lasers and Electro-Optics, Technical digest (Optical Society of America, 2007), paper CTuN1.

[21] Payne, S.A., Chase, L.L., Smith, L.K., Wayne L. K., and Krupke W.F., IEEE J. Quant. Elect. 28 (1992) 26192630.

[22] Schweitzer,T., Jensen, T., Heumann, E., Huber, G.,Optics Communications 118 (1995) 557.

[23] Tanabe, S., Suzuki,K., Soga,N. and Hanada,T., "Mechanisms and concentration dependence of Tm^{3+} blue and Er^{3+} green up-conversion in codoped glasses by red-laser pumping," J. Lumin. 65, 247-255 (1995).

[24] Jenkins, N., Bowman, S. R. , O'Connor, S., Searles, S. K. and Ganem, J.,"Spectroscopic characterization of Er doped KPb_2Cl_5 laser crystals," Opt. Mater. 22, 311-320 (2003).

[25] A. Braud, S. Girard, J. Doualan, and R. Moncorge, "Spectroscopy and Fluorescence Dynamics of (Tm^{3+},Tb^{3+}) and (Tm^{3+},Eu^{3+}) Doped $LiYF_4$ Single Crystals for 1.5 μm Laser Operation, " IEEE Journal of Quantum Electronics, 34, 2246-2255 (1998).

[26] E. Roman, M. Hempstead, C. Ye, S. Nouh, P. Camy, P. Laborde,C. Lerminiaux, 1.7 μm Excited State Absorption Measurement in Erbium-Doped Glasses," Appl. Phys. Lett. 67 (1995) 470.

[27] D. L. Dexter, J. Chem. Phys. 21 836 (1953).

[28] T. Förster, Disc. Faraday Soc. 27 7 (1959).

[29] A. G. Okhrimchuk, L. N. Butvina, E. M. Dianov, N. V. Lichkova, V. N. Zagorodnev, and A. V. Shestakov **36**(2006) 41.

[30] M. Inokuti and F. Hirayama, J. Chem. Phys. **43** (1965) 1978.

[31] Amedzake, Peter. 2008.Crystal Growthand Spectrosocopic Characterizationof $Pr^{3+}$and Dy^{3+} Doped $KPb_2Br_5$and KPb_2Cl_5 For Mid-Infrared Laser Applications. PhD Dissertation, Hampton University.

[32] Zhou Ya-xun, XU Xing-Chen, Chen Fen, Lin Jian-hui, and Yang Gaobo, Optoelectronics Letters **8** (2012) 0273.

[33] A. Ferrier, M. Velazquez, J. L. Doualan, and R. Moncorge, J. of AppL. Phys. 104 (2008) 123513.

[34] R. Balda, M. Voda, M. Al-Saleh, J. Fernandez, Journal of Luminecence **97** (2002) 190.

[35] A.G. Okhrichuk, I. V. Shestakova, N. V. Lichkova, V. Zagoridnev, and K. N. Boldyrev, Advanced Solid State Laser Conference (Optical Society of America, 2008), paper WE6.

[36] A.G. Okhrichuk, L. N. Botvina, E. M. Dianova, N. V. Lichkova, V. Zavgorodnev, and A. V. Shestakov, Advanced Solid State Laser Conference (Optical Society of America, 2007), paper WB3.

[37] R. Balda, J Fernandez, A. Mendioroz, M. Voda, and M. Al-Saleh, Optical Materials **24**(2003) 91.

[38] T. Schweizer, T. Jensen, E. Heumann, G. Huber, Optics Communications **118** (1995) 557.